



1 **Impact of Asian aerosols on the summer monsoon strongly**
2 **modulated by regional precipitation biases**

3

4

5 Zhen Liu^{1,2}, Massimo A. Bollasina², Laura J. Wilcox³

6

7 ¹Earth, Ocean and Atmospheric Sciences (EOAS) Thrust, Function Hub, The Hong Kong University of Science and
8 Technology (Guangzhou), Guangzhou, China

9

10 ²School of Geosciences, University of Edinburgh, UK

11

12 ³National Centre for Atmospheric Science, Department of Meteorology, University of Reading, Reading, UK

13

14 Correspondence to Zhen Liu (henryzhenliu@hkust-gz.cn)

15

16

17



18 **Abstract.** Reliable attribution of Asian summer monsoon variations to aerosol forcing is critical to reducing uncertainties
19 in future projections of regional water availability, which is of utmost importance for risk management and adaptation
20 planning in this densely populated region. Yet, simulating the monsoon remains a challenge for climate models which
21 suffer from long-standing biases, undermining their reliability in attributing anthropogenically-forced changes. We
22 analyse a suite of climate model experiments to identify a link between model biases and monsoon responses to Asian
23 aerosols, and the physical mechanism underpinning this link, including the role of large-scale circulation changes. The
24 aerosol impact on monsoon precipitation and circulation is strongly influenced by a model's ability to simulate the spatial
25 distribution and temporal variability of the climatological monsoon winds, clouds and precipitation across Asia, which
26 critically modulates the magnitude and efficacy of aerosol-cloud-precipitation interactions, the predominant driver of the
27 total aerosol response. There is a strong interplay between South and East Asia monsoon precipitation biases and their
28 relative predominance in driving the overall monsoon response. We found a striking contrast between the early and late
29 summer aerosol-driven changes ascribable to opposite signs and seasonal evolution of the biases in the two regions. A
30 realistic simulation of the evolution of the large-scale atmospheric circulation is crucial to realise the full extent of the
31 aerosol impact over Asia. These findings provide important implications to better understand and constrain the diversity
32 and inconsistencies of model responses to aerosol changes over Asia in historical simulations and future projections.

33

34 **1 Introduction**

35 The Asian summer monsoon is one of the key components of the global atmospheric circulation, providing critical water
36 resources to more than 60% of the world's population. Because of this reliance, even small changes in the spatio-temporal
37 characteristics of the monsoon represent a significant hurdle for the local population. Yet, despite considerable efforts,
38 simulating the monsoon remains a long-standing challenge for climate models as some biases have persisted for decades,
39 such as the deficient rainfall over central India and excess wetting over eastern China (Sperber et al., 2013; Liu et al.,
40 2021). The existence of these large and widespread biases not only decreases the confidence in the modelled monsoon
41 and associated physical mechanisms (Yang et al., 2019; Jiang et al., 2020; Rajendran et al., 2022; Liu et al., 2022) but
42 also represents a major cause of the large inter-model spread in historical monsoon evolution (Zhou et al., 2019; Guilbert
43 et al., 2023). Moreover, these biases are likely to hinder reliable monsoon projections with critical implications for water
44 management and planning across Asia and subsequent impacts on agriculture and economy (Zhou et al., 2019; Cao et al.,
45 2020; Wang et al., 2020; Pillai et al., 2021). In particular, model biases introduce large uncertainties in our ability to
46 separate externally-forced from internally-generated monsoon variability, preventing robust attribution of rainfall changes
47 to specific drivers, including the extent to which recent and near-future trends are driven by anthropogenic aerosols
48 (Wilcox et al., 2015; Dai et al., 2022).



49

50 Anthropogenic aerosols represent the largest uncertainty in quantifying the total anthropogenic forcing on climate since
51 the pre-industrial era (Andrews and Forster, 2020). Aerosols exert an overall cooling effect on climate by modulating
52 solar radiation via absorption and scattering, as well as by acting as cloud condensation and ice nuclei and thus altering
53 cloud albedo and lifetime and precipitation processes (Boucher et al., 2013). Asia has the largest present-day
54 anthropogenic aerosol burden as rapid urbanization and economic development have drastically increased aerosol
55 emissions and loading since the 1950s (Lin et al., 2016a). China has recently implemented strong pollution control policies,
56 which has substantially reduced aerosol emissions since 2013 (e.g., 59% for sulfur dioxide and 28% for black carbon
57 during 2013–2017; Zheng et al., 2018). Yet, Asia will still experience the highest aerosol loading in the world over the
58 coming decades as projected by the different future socioeconomic pathways used in the Coupled Model Inter-comparison
59 Project Phase 6 (Lund et al., 2019).

60

61 Aerosols have been found to play a key role in driving the observed decreasing trend in Indian summer rainfall (Chung
62 and Ramanathan, 2006; Lau and Kim, 2010; Bollasina et al., 2011; Guo et al., 2015) and the southern-flood-northern-
63 drought (SFND) pattern over East Asia (Menon et al., 2002a; Guo et al., 2013; Song et al., 2014a; Yu et al., 2016; Tian
64 et al., 2018) during the late 20th century. Studies that have separately investigated the impact of regional (Asian) and
65 remote (outside Asia) emissions have found the former to be fundamental to explaining the observed monsoon changes,
66 but with the latter also providing an important contribution (Cowan and Cai, 2011; Ganguly et al., 2012; Bollasina et al.,
67 2014; Dong et al., 2016). In particular, South and East Asian aerosols separately exert a strong influence on both the
68 South and East Asian monsoons, with contrasting, if not opposite, changes as well as strong non-linear interactions
69 between the responses to individual emission sources (Singh et al., 2019; Sherman et al., 2021; Herbert et al., 2022; Liu
70 et al., 2023).

71

72 At larger scale, the Asian monsoon march is linked to the evolution of semi-permanent features of the tropical and
73 extratropical atmospheric circulation, such as the western Pacific subtropical high (Zhang et al., 2005) and the Mascarene
74 high in the southern Indian Ocean (Vidya et al., 2020). The monsoon and the large-scale circulation are affected by
75 anthropogenic aerosol forcing, resulting in complex and intertwined interactions between externally and internally forced
76 variability (Deser et al., 2012; Huang et al., 2020a; Zha et al., 2022). Understanding the interplay between the Asian
77 monsoon and the large-scale circulation outside Asia and the extent to which concurrent changes in the large-scale
78 circulation modulate the monsoon response to regional aerosol changes is thus beneficial to achieve better monsoon
79 simulations and more robust projections (An et al., 2012; Liu et al., 2021).

80



81 One approach that has provided valuable insights into the mechanisms of aerosol-monsoon interactions is the
82 decomposition of the response into two complementary components: a fast response involving atmospheric and land
83 surface adjustments but fixed sea surface temperature (SST), acting on a short time scale (few years), and a slow response
84 scaling with SST changes (Samset et al., 2016; Li et al., 2020; Zhang et al., 2021). The fast and slow components over
85 and around Asia show similar features under global and regional (Asian only) aerosol forcing. In the case of sulfate
86 aerosols, the total response over Asia and downwind Pacific regions shows substantial precipitation decreases, with the
87 fast component featuring negative anomalies over land and positive ones over the adjoining ocean. While the monsoon is
88 a fully atmosphere-ocean coupled system, recent studies have found rapid adjustments to be of fundamental importance
89 in explaining inter-model differences in the aerosol response (Fläschner et al., 2016; Liu et al., 2018; Zanis et al., 2020).
90 Building on the above considerations, this study aims to identify a link between model biases and monsoon response to
91 Asian aerosols, and the underpinning physical mechanism, including the role of large-scale circulation changes outside
92 Asia and SST changes. The rest of the manuscript is organized as follows: Details of model experiments and analysis
93 methods are provided in Section 2. Section 3 examines the influence of precipitation biases on the climate response to
94 Asian aerosol perturbations and describes the underlying mechanism. Conclusions follow in Section 4.

95 **2 Data and methods**

96 The primary dataset analysed consists of simulations conducted with the Met Office Unified Model (MetUM) HadGEM3-
97 Global Atmosphere version 7.1 (GA7.1) at N96 horizontal resolution ($1.875^\circ \times 1.25^\circ$) and with 85 vertical levels
98 extending up to 85 km (Walters et al., 2019). The GLOMAP modal aerosol scheme is used to represent aerosol processes,
99 including a representation of both aerosol-radiation and aerosol-cloud interactions (see Mann et al., (2010) and Bellouin
100 et al. (2013) for more details). GA7.1 was used as the atmospheric component of the climate model participating in
101 CMIP6. Compared to the previous model version (GA7.0), GA7.1 has a smaller global-mean anthropogenic aerosol
102 effective radiative forcing (Walters et al., 2019).

103

104 A set of four experiments (see Table 1) is performed with GA7.1 for the period December 1991 to December 2012 with
105 prescribed daily observed SST from the European Centre for Medium-Range Weather Forecasts (ECMWF) Interim Re-
106 Analysis (Dee et al., 2011). The reference experiment (CONT) is driven by monthly-varying historical emissions of
107 anthropogenic aerosols and precursors following CMIP6 (Hoesly et al., 2018). CONTfA is identical to CONT except for
108 having anthropogenic aerosol emissions of sulfur dioxide (SO₂), black carbon, and organic carbon and biomass burning
109 emissions fixed at the year 1991 over Asia (10° – 45° N, 60° – 125° E, the purple box in Fig. 1c). The difference between
110 CONT and CONTfA represents the fast response to changes in Asian anthropogenic aerosols.



111 To separate regional and remote circulation adjustments to aerosol forcing, dynamical nudging (also known as Newtonian
112 relaxation) is applied by constraining horizontal winds towards ERA-I (Kooperman et al., 2012; Liu et al., 2021). We
113 conducted another pair of experiments (NUDG and NUDGfA, respectively) identical to CONT and CONTfA except for
114 nudging horizontal winds to ERA-I outside Asia (the region outlined in Fig. 1c). The difference, NUDG minus NUDGfA,
115 represents the local response to Asian aerosols in the absence of concurrent changes in the large-scale atmospheric
116 circulation outside Asia. Nudging is only applied above the planetary boundary layer (model level 12, or approximately
117 850 hPa) so that low-level winds can adapt to surface conditions (e.g., different topography with respect to ERA-I; (Liu
118 et al., 2021)). Comparing the differences between the free-running experiments (i.e., CONT – CONTfA) and the nudged
119 runs (i.e., NUDG – NUDGfA) enable us to determine the extent to which simultaneous adjustments in the large-scale
120 atmospheric circulation outside the region modulate the Asian monsoon response to changes in regional anthropogenic
121 aerosols. To account for the role of internal variability, all experiments consist of three ensemble members initialized
122 from different atmospheric conditions. Only the last 10 years of each experiment are analysed (i.e., 2003 – 2012) when
123 Asian aerosol emissions are at the maximum (Fig. 1a). The results are however largely unchanged if a longer analysis
124 window is chosen (e.g., 15-year averages) as anomalies display similar large-scale features, albeit of slightly smaller
125 magnitude (not shown). The statistical significance of ensemble-mean differences relative to model internal variability is
126 estimated using a 35-year HadGEM3-GA7.1 experiment where all forcing factors are set at pre-industrial (1850) levels.
127 After splitting the output from this simulation into 26 overlapping 10-year segments, the probability distribution of the
128 unforced 10-year means for a 3-member ensemble is computed by randomly selecting three of these segments without
129 repetition, for a total of 2600 samples. In turn, the probability distribution of the 10-year ensemble-mean differences is
130 calculated by randomly selecting two of the 2600 samples a total of 10000 times (e.g., Efron and Tibshirani, 1993), and
131 the 90% confidence interval is estimated as the range in which 90% of the samples fall.

132
133 Data from the Precipitation Driver Response Model Intercomparison Project (PDRMIP; Samset et al., 2016) is also
134 utilized to corroborate our findings from a multi-model perspective. Two experiments are considered: the baseline
135 simulation forced by present-day (year 2000) levels in aerosols and greenhouse gases emissions/concentrations, and one
136 identical to the baseline run except for having a ten-fold increase in sulfate aerosol emissions/concentrations over Asia
137 (10°–50°N, 60°–140°E). The geographical distribution of the baseline sulfate burden in the PDRMIP ensemble (Myhre
138 et al., 2017) is very close to that in the CONT-CONTfA difference (Fig. 1b) over Asia, with the latter also showing an
139 approximately 10-fold increase in SO₂ emissions since the early 1990s (Fig. 1a), which ensures a sound comparison
140 between the different simulations. The PDRMIP experiments were run for 15 years with fixed present-day SSTs and for
141 100 years in coupled mode ((Liu et al., 2018). The response to Asian aerosols is identified as the difference between the
142 perturbed and baseline simulation averaged over the years 6–15 for both fixed SST and coupled simulations. In the case
143 of fixed SST, this choice is consistent with previous studies (Samset et al., 2016; Myhre et al., 2017) and accounts for the



144 adjustment time to the step change in emissions from the baseline simulation. We chose the same averaging period also
145 for the coupled experiments for consistency with the nature of the transient response to time-evolving emissions examined
146 in this study. In this sense, the coupled experiments allow us to ascertain whether the findings are sensitive to “fast”
147 oceanic-mediated responses (i.e., air-sea interactions), thus excluding the contribution brought about by slow (i.e., multi-
148 decadal) oceanic adjustments pertaining to a fully equilibrated atmosphere-ocean climate system.

149

150 We also analyse the transient historical simulations with the MetUM HadGEM3-GC2 coupled model described in (Wilcox
151 et al., 2019). These consist of four-member ensemble runs with all historical forcings, and a companion experiment in
152 which aerosols over Asia (5° – 47.5° N, 67.5° – 145° E) are fixed at their 1971–1980 mean levels. The difference between
153 the two ensemble means across two 10-year periods (i.e., 1999–2008 and 1971–1980) is interpreted as the total transient
154 response to Asian aerosol changes. We choose the later period 1999–2008 when aerosol emission differences maximize
155 (see Fig. 1 in Wilcox et al., 2019) and are at a comparable magnitude to our HadGEM3-GA7.1 simulations. These
156 experiments allow us to ascertain the consistency between uncoupled and coupled transient settings.

157

158 In light of the strong seasonality of the precipitation response to aerosol changes and the partial compensation between
159 the monsoon response in the early and late summer (Bollasina et al., 2013), we examine monthly precipitation and
160 circulation changes in addition to the June–September seasonal means. The simulated climatological precipitation and
161 circulation are evaluated against the arithmetic mean of the Climate Prediction Center Merged Analysis of Precipitation
162 (Xie and Arkin, 1997) and the Global Precipitation Climatology Project (GPCP) version 2 (Adler et al., 2003)
163 precipitation observations (Wang et al., 2014) and the ECMWF Reanalysis v5 (Hersbach et al., 2020) sea-level pressure
164 and 850-hPa winds for the period 1981–2010, respectively. These datasets are also used to provide a broader interpretation
165 of the aerosol-driven simulated changes in the context of recent observed trends.

166 **3 Results**

167 **3.1 Monsoon response to Asian aerosols**

168 The temporal evolution of the seasonal-mean differences in aerosol emissions and total aerosol optical depth (AOD)
169 between CONT and CONTfa averaged over Asia (the area enclosed by the purple box in Fig. 1c) is displayed in Fig. 1a.
170 The rapid rise of AOD after 2002 is mostly due to the increase in SO₂ emissions as the similarity between the respective
171 time-series indicates. BC and OC emissions exhibit a comparatively minor increasing trend, while biomass burning
172 emissions show negligible changes. The spatial distribution of changes in column-integrated sulfate burden closely
173 resembles that of emission changes and is characterized by large increases over eastern China and northern India (Fig.



174 1b). The pattern of the seasonal AOD change follows that of sulfate loading, further indicating the primary contribution
175 of SO₂ emissions to the total aerosol amounts over the region. Positive AOD anomalies also extend eastward from China
176 to the northwestern Pacific, reflecting atmospheric transport of aerosols by climatological southwesterly winds. Seasonal
177 mean aerosol changes across Asia are thus dominated by sulfate aerosols, consistently with longer-term trends since the
178 1950s (Lund et al., 2019), which hints at a predominant role of SO₂ emissions in driving the response discussed below.

179
180 Fig. 2a shows the aerosol-driven summer precipitation changes. A band of excess rainfall stretches from southeastern
181 China and the South China Sea (SCS) across northern Indochina and the northern the Bay of Bengal (BOB) to northern
182 India, associated with a negative sea-level pressure anomaly and anomalous cyclonic flow centered over the northern
183 BOB (Fig. 2b). The simultaneous northwestward shift and strengthening of the Mascarene High over the equatorial Indian
184 Ocean leads to an enhanced cross-equatorial southwesterly flow over the western tropical Indian Ocean and subsequent
185 north-equatorial eastward moisture transport and precipitation increase across the basin (Fig. 2b and 2c), indicating an
186 intensified monsoon circulation. The anomalous wind then turns anticlockwise, bringing abundant moisture across the
187 BOB to northern India, Indochina, and southern China (Fig. 2c). Concurrently, anomalous dry westerlies over central
188 India lead to precipitation decrease, resulting in an approximately southwest to northeast oriented wet/dry rainfall dipole.

189
190 Over China, the widespread wetting to the south, together with the drying to the north, form a meridional dipole. The
191 dipole is accompanied by a marked anomalous anticyclone centered over the western subtropical Pacific and extending
192 further inland, suggesting a strong dynamical link with the rainfall anomalies via modulation of the climatological western
193 Pacific subtropical high (WPSH; Fig. 2a and 2b). On the southwestern flank of the anticyclone, anomalous southeasterlies
194 blow from the sub-tropical western Pacific across SCS and bring moisture to southern China (Fig. 2c). Here the flow
195 converges with the southwesterly winds from the Indian Ocean mentioned above, resulting in the abundant precipitation
196 increase. Moist southerlies further extend over eastern China and result in a positive, albeit of weak magnitude, moisture
197 convergence anomaly. This contrasts with the local precipitation deficit which, given also the modest evaporation
198 anomaly (not shown), appears to be associated with moisture divergence due to transient eddies whose contribution to
199 the total moisture flux convergence is relevant for the region (e.g., Seager et al., 2010; Li et al., 2018).

200
201 Examining these changes in a broader context, the aerosol-driven rainfall pattern displays, in its large-scale features, a
202 remarkable similarity, but opposite sign, to observations (Fig. S1). In particular, model and observations feature key
203 rainfall action centers of comparable magnitude and in similar geographical locations while of opposite polarity. For
204 example, observed changes show drying from northern India across the northern BOB to southeastern China, with wetting
205 over central and western India, northern China, and the western subtropical Pacific (Fig. S1a), in stark contrast to the
206 simulated anomalies shown in Fig. 2a. These precipitation anomalies over East Asia are associated with an anomalous



207 cyclone over the western subtropical Pacific (Fig. S1b; compared to the anomalous anticyclone in Fig. 2), leading to
208 oceanic moisture advection over northern China and dry northeasterlies over southern and eastern China. Anomalous
209 anticyclonic anomalies are seen over the northern BOB in contrast to a low over the Arabian Sea, which leads to excess
210 rainfall over central and western India and a deficit to the northeast and the northern BOB (opposite to the simulated
211 dipole in Fig. 2). Interestingly, the consistency between observed and simulated (sign-reversed) precipitation and sea-
212 level pressure patterns is also evident in CONT (Fig. S1c and S1d), albeit with some dissimilarities over land, while it is
213 less obvious when aerosol emissions are not evolving (Fig. S1e and S1f), particularly around the Indian subcontinent and
214 eastern China, resulting in an overall mixed signal. While this suggests a possible important role of aerosols in driving
215 the model anomalies, the opposite polarity of the aerosol-induced patterns compared to observations is puzzling and
216 warrants further investigation into the underpinning cause and physical mechanism.

217
218 Inspection of monthly precipitation and low-level circulation changes reveals a stark contrast over the Indian subcontinent
219 and adjacent ocean between the early and late monsoon season: increased precipitation and anomalous cyclonic flow over
220 the BOB in June, consistent with the seasonal mean, and decreased precipitation and anomalous anticyclonic winds over
221 India in September (Figs. S2 and S3). Rainfall and circulation anomalies in July display similarities to those in June, while
222 August shows a mixed pattern, with more spatially confined and smaller magnitude anomalies. Over East Asia, the June-
223 July precipitation anomalies, closely resembling the seasonal-mean changes, feature a zonal-elongated meridional dipole,
224 with wetting stretching from Indochina and southern China to the South China Sea, and drying to the north across central
225 and eastern China. Interestingly, the dipole reverses sign in September, accompanied by a southward displacement (i.e.,
226 the dipole nodal line moves from around 30°N to about 20°N), with widespread drying over southern Indochina and most
227 of the western subtropical Pacific and wetting to the north over northern Indochina and most of China. Consistently with
228 the comparison for the seasonal means, the sub-seasonal aerosol-driven simulated response patterns bear a strong
229 similarity, with opposite signs, to those observed (not shown).

230
231 These contrasting changes in the simulated aerosol-induced responses between the early and late summer, despite
232 negligible monthly variations in magnitude and spatial distribution of aerosol emissions across Asia, especially for SO₂
233 (not shown), and the consistently reversed polarity of their key centres compared to observations, suggest that different
234 mechanisms may underpin the responses throughout the season. This also suggests a possible link between long-term
235 changes and the underlying mean seasonal cycle, and the possibility of discrepancies between simulated and observed
236 characteristics in the latter to be the cause of the differences in the former. From a more general perspective, this also
237 highlights the importance of investigating and interpreting seasonal monsoon changes accounting for the pronounced sub-
238 seasonal variability in the response – an aspect usually overlooked in aerosol-monsoon research but particularly relevant
239 for attribution studies.



240 3.2 A mechanism linking model climatology to response

241 The accuracy of the simulated regional climate change signal and its attribution to anthropogenic drivers have been
242 suggested to be strongly dependent on the model performance in reproducing the corresponding mean climatological
243 conditions, which represent the baseline state on top of which changes occur (Matsueda and Palmer, 2011; Christidis et
244 al., 2013). Indeed, a link between model bias and corresponding response has been shown to hold, for example, in the
245 case of summer precipitation over Asia (Wilcox et al., 2015), global SST patterns and overlying rainfall changes (He and
246 Soden, 2016), tropical rainfall (Chadwick, 2016) and circulation (Zhou and Xie, 2015) extratropical stationary eddies and
247 their influence on tropical convection (Chen et al., 2018) and Arctic Ocean temperature (Park and Lee, 2021). Given that
248 state-of-the-art climate models still suffer from large and persistent biases in simulating magnitude and distribution of the
249 monsoon precipitation and circulation across Asia (Wilcox et al., 2020; Rajendran et al., 2022; Tong et al., 2022), it is
250 certainly plausible for these biases to exert a sizeable control on the aerosol-induced monsoon changes. Climatological
251 biases in climate models could lead to unrealistic projections of anthropogenic climate change and add further
252 uncertainties, for example due to their possible non-stationarity (Krinner and Flanner, 2018). Examining the sub-seasonal
253 evolution of the model bias could therefore provide insights into the simulated aerosol-induced monsoon response
254 described above, a topic that has been insufficiently addressed and possibly underappreciated so far.

255
256 Fig. 3a and 3b show the model precipitation bias relative to the mean of CMAP and GPCP in June and September,
257 respectively. In June, there is a clear anomalous meridional dipole over the Indian sector with rainfall excess over the
258 equatorial Indian Ocean and deficit over India and surrounding oceanic areas, including the BOB (Fig. 3a). This dipole
259 pattern is similar to that of the seasonal-mean bias commonly presented in both uncoupled and coupled models (Song and
260 Zhou, 2014; He et al., 2022; Rajendran et al., 2022). Particularly, the magnitude of the June dry bias over the Indian
261 subcontinent (-2.8 mm day^{-1}) is about 60% of the observed climatological amount (4.7 mm day^{-1}). The model is
262 excessively wet to the east over northern Indochina and most of China, particularly to the south, with predominant dry
263 anomalies over the China Sea. Interestingly, this bias pattern over continental Asia, and particularly the contrasting dipole
264 between (dry) India and (wet) northern Indochina/China, bears a close resemblance, with opposite sign, to the June
265 aerosol-induced simulated precipitation distribution discussed above (wetting over India and drying over northern
266 Indochina/China; Fig. 3b). Is there a mechanistic link between bias and aerosol-driven response?

267
268 Aerosol-cloud interactions have been found to play a fundamental role in modulating the Asian summer monsoon
269 response to anthropogenic aerosols, both in uncoupled and coupled experiments (Guo et al., 2015; Li et al., 2018).
270 Hydrophilic aerosols (e.g., sulfate) activated at a given supersaturation level can serve as cloud condensation nuclei and
271 increase the cloud droplet number concentration (CDNC). At constant cloud liquid water content, the increases in CDNC



272 reduce the cloud effective radius and enhance the cloud albedo (Twomey, 1974), exerting a cooling effect at the surface.
273 Meanwhile, the smaller cloud droplets reduce the collision/coalescence probability of droplets and thus weaken the
274 precipitation efficiency (Albrecht, 1989). Cloud effective radius, the critical variable linking aerosol emission changes to
275 cloud and precipitation variations, is proportional to the liquid water content at a given CDNC (Menon et al., 2002b).
276 While column water content also changes in response to aerosol variations (Sato et al., 2018; Wang et al., 2022), and thus
277 cause and effect are tightly intertwined at short time scales, the above hints at the possibility of baseline conditions to
278 modulate aerosol-cloud interactions and the subsequent monsoon response to aerosol changes, especially in the presence
279 of large model discrepancies in simulating the climatological distribution of atmospheric moisture (John and Soden, 2007;
280 Bastin et al., 2019; Han et al., 2022). The marked and abrupt shift in the atmospheric state accompanying the monsoon
281 onset and subsequent establishment across Asia is also by nature substantially affected and pre-conditioned by the
282 presence of anomalous conditions in the preceding spring months. In view of this and to better identify possible precursor
283 conditions leading to the marked aerosol-induced response in June, we examine the model anomalies in late spring.

284

285 It is worth noting that while the band of excess climatological rainfall over southern and eastern China is present for most
286 of the year, the magnitude of the bias undergoes a rapid increase from April until the peak in June and then decays from
287 July to September (Fig. S4). Also, the wet bias over eastern China is particularly spatially extensive in the spring (up to
288 50% of the climatology), while a weak, dry anomaly appears in the summer over the lower reaches of the Yangtze River.
289 Importantly, the widespread wet anomaly over China in April–May is largely collocated with the largest aerosol emission
290 sources, particularly SO₂ (Fig. S5a). The excess climatological moisture available over China provides favourable
291 conditions for the aerosol impact via aerosol-cloud interactions in addition to changes in radiation. In fact, the CONT–
292 CONTfA difference shows reduced shortwave clear-sky radiation at the surface, a simultaneous increase in cloud droplet
293 number concentration, and a decrease of the cloud-top effective radius (Fig. S5b–d). An anomalous anticyclone situated
294 over southeastern China (Fig. S5h), consistent with the pattern of aerosol forcing, leads to a meridional dipole in the water
295 content and precipitation response, with large and widespread wet anomalies over Indochina and the SCS and drying over
296 eastern China (Fig. S5e and S5f).

297

298 Conversely, the model underestimates the observed rainfall over the already dry pre-monsoon Indian subcontinent, with
299 a substantial dry bias over eastern India and the BOB (Figs. S4a and S4b). In response to the aerosol increase, there is a
300 clear reduction in clear-sky shortwave radiation over India, albeit secondary to that over China due to the smaller emission
301 changes, and a minor increase (decrease) in cloud droplet number concentration (cloud top effective radius) (Fig. S5b–
302 d). This indicates overall weak aerosol-radiation and aerosol-cloud interactions, resulting in negative, although very weak,
303 precipitation anomalies and associated mixed lower-tropospheric circulation response (Fig. S5f and S5h). It is worth
304 noting that the upper-level divergent outflow from the rainfall maximum anomaly over Indochina converges over



305 northeastern India where it subsides and generates a near-surface return flow, forming a system of closed and interacting
306 cells (Fig. S5g and S5h).

307

308 With the arrival and establishment of the monsoon over Asia in June, the simulated climatological precipitation increases
309 considerably over northern Indochina and southern China but only marginally over India (Fig. S6), resulting in a
310 substantial zonal precipitation dipole in the model bias across Asia, with marked dry anomalies over and around India
311 and wet conditions over Southeast Asia and southern China (Fig. 3a). There is also a dry anomaly over eastern China,
312 resulting from weak southwesterlies and stagnation of the monsoon front to the south (Liu et al., 2021). As in the spring,
313 the patterns of the precipitation bias and associated water content anomalies are important to understand the corresponding
314 aerosol-driven response. The anticyclonic circulation anomaly over eastern China strengthens and widens compared to
315 the earlier months from both aerosol-radiation and aerosol-cloud interactions (Fig. 3c and S5h), manifested in the
316 considerable reduction in surface clear-sky shortwave radiation (Fig. S7c), overall increased cloud droplet number
317 concentration, and decreased cloud effective radius over central and eastern China (Fig. 4a and 4b). Note the latter displays
318 positive anomalies over southern China, where enhanced easterlies along the southern flank of the anticyclone bring
319 moist-laden air from the western Pacific towards South Asia (Fig. 3c), leading to increased water availability and the
320 large precipitation excess there. Over India, the substantial climatological atmospheric water content deficit, seen in the
321 ensuing large dry bias (Fig. 3a), strongly limits local aerosols to exert a sizable impact by markedly weakening the
322 magnitude of regional aerosol-cloud interactions (e.g., modest changes in cloud top effective radius in Fig. 4b). Regional
323 anomalies in the aerosol response are thus interpreted as remotely-induced by the large-scale circulation adjustment to
324 aerosol changes over China. Local aerosols and ensuing circulation and precipitation response are therefore tightly
325 coupled over Asia and linked by positive feedbacks, whereby an initial aerosol-induced anomaly in precipitation
326 subsequently acts to reinforce the anomalous pattern by regional circulation adjustments. For example, the deep ascent
327 and upper tropospheric divergent outflow associated with the excess precipitation over the BOB and Indochina bifurcates
328 with the primary branch converging and subsiding over northeastern China (reinforcing the local anticyclone) and the
329 secondary branch over the southeastern Philippines Sea where dry anomalies are found and are part of the northwestward
330 rainfall shift (Fig. S8a–c).

331

332 As summer progresses, the simulated climatological precipitation reaches its peak over India, while it retreats markedly
333 over China (Fig. S7a and S7b). This, together with the anomalies set up as part of the aerosol response in the earlier part
334 of the season (Fig. 3b), leads to enhanced moisture availability over South Asia compared to the earlier months, while
335 also partially alleviating the reduced, but persisting, model dry bias there (Fig. 3e). Conversely, over China, the moisture
336 deficit from the aerosol-weakened monsoon circulation (Fig. 3b), as well as the rapid monsoon demise in the simulated
337 climatology (Fig. S7e), contribute to lessening the degree of interaction between aerosols and clouds and precipitation.



338 As a result, aerosol-cloud interactions over South Asia are more effective compared to the early summer, and the
339 continental-scale simulated response is predominantly driven by aerosol-induced anomalies over South Asia. Associated
340 with a decrease in cloud top effective radius (Fig. 4f), negative precipitation anomalies appear over South Asia from
341 August (Fig. S3c), with maximum peak in September (Fig. 3f). Correspondingly, the lower-tropospheric circulation
342 features an anomalous anticyclone, with westerly winds over northern India and the BOB (Fig. 3g). The flow turns
343 southwesterly over northern Indochina, bringing more moisture to eastern China (leading to increased cloud top effective
344 radius in Fig. 4f) and increasing precipitation which forms a zonal dipole with the rainfall decrease over the north-
345 equatorial western Pacific (Fig. 3f and 3h). The associated anomalous western Pacific anticyclone weakens and shifts
346 eastward (Fig. 3g). The large-scale anomalous circulation pattern is characterized by the mid-tropospheric vertical motion
347 and divergent outflow over southern China, and upper-level convergence and subsidence over South Asia and the north-
348 equatorial western Pacific (Fig. S8d–f), which further attests for the strong coupling across the region.

349 3.3 Aerosol response in nudged simulations

350 The Asian monsoon response to aerosol changes discussed above entails large-scale atmospheric circulation adjustments
351 extending beyond the Asian region. It is therefore interesting to understand whether and the extent to which they
352 contribute to driving the regional response. Constraining the large-scale circulation outside Asia to observations allows
353 us to isolate the effect of remote (i.e., outside Asia) circulation changes in generating the monsoon response to Asian
354 aerosols.

355
356 The AOD differences between the pair of nudged simulations (Fig. S9) resemble those shown in Fig. 1 despite the
357 considerably different circulation and precipitation anomalies (see Fig. 3c, 3g, 5c, 5g), indicating that the AOD
358 distribution is predominantly influenced by emissions changes rather than by aerosol transport and removal processes.
359 The spatial patterns of both the June and September precipitation biases in NUDG, where horizontal winds outside Asia
360 are nudged to ERA-I, are overall very similar to those in the control simulation (cf. Fig. 5a and 5e). Sub-regional
361 differences in the magnitude of the bias between the two sets of experiments are however noticeable (e.g., the dry bias is
362 markedly reduced over India, whereas southeastern China is wetter, compared to CONT), indicating that an improved
363 representation of the remote circulation can potentially reduce the precipitation bias in some areas but not necessarily
364 across the entire domain (Liu et al., 2021).

365
366 The June precipitation response to aerosol changes features an approximately meridional dipole, with widespread drying
367 from north-eastern India to southern China and wet anomalies over central India, the BOB, and parts of the South China



368 Sea (Fig. 5b). Compared to the free-running simulations, precipitation anomalies are of much smaller magnitude and
369 mostly confined within Asia and the neighbouring oceanic areas, without a significant aerosol signature downstream (e.g.,
370 over the equatorial Indian Ocean and the subtropical Pacific). This is expected as the atmospheric circulation above the
371 planetary boundary layer is nudged outside Asia, and attests to the key role of large-scale circulation adjustments in
372 realizing the aerosol impact. Consistently with the link between rainfall bias and response to aerosol forcing found in the
373 free-running simulations, wetter climatological conditions over China and a reduced dry bias over India translate into
374 more efficient aerosol-cloud interactions over both regions (Fig. 5a). As a result, the ensuing precipitation response, while
375 bearing similarities with that in Fig. 3 and thus on the driving role of Chinese aerosol emissions, also shows noticeable
376 differences: the drying over China is more spatially extensive, particularly to the south, while the wetting over the Indian
377 sector is mainly confined to the northern BOB (Fig. 5b). While sign and pattern of the aerosol-induced response are
378 consistent with the bias pattern, the generally weak anomalies are a result of the unchanged large-scale circulation outside
379 Asia in the nudged experiments. For example, Fig. 5c shows a pattern of sea level pressure anomalies which resembles
380 that shown in Fig. 3c, but with much smaller gradients and mostly confined to Asia only. In particular, there is only a
381 very weak westerly flow across the north-equatorial Indian Ocean, with reduced moisture supply towards Indochina and
382 southern China, in contrast to the vigorous cross-equatorial moisture-laden flow from the western Indian Ocean in the
383 free-running experiments. These anomalies, manifestation of a *local* aerosol effect, are indicative of the predominant role
384 of large-scale circulation adjustments and two-way interactions with local anomalies in realising the full extent of the
385 aerosol impact over Asia. Nudging the circulation outside Asia thus proves to be a strong constraint on the model response
386 to aerosols over Asia, despite unchanged emissions compared to the free running simulations.

387

388 In September, the dry bias over India is reduced compared to June (Fig. 5e) as in the free-running simulation. The wet
389 bias over China also reduces overall in magnitude compared to June, although NUDG is wetter than CONT (Fig. 1b),
390 which may be conducive to enhanced aerosol-cloud interactions. In fact, CDNC increases across Asia (Fig. S10c) but
391 cloud top effective radius decreases mainly over central and eastern China, with conversely muted changes over India
392 (Fig. S10d). As a result, precipitation decreases over most of central and eastern China, accompanied by positive sea-
393 level pressure anomalies and anomalous low-tropospheric anticyclonic circulation (Fig. 5f and 5g). The anomalous
394 easterly flow over northern Indochina and northern India draws anomalous southwesterly moisture transport across India,
395 which features widespread wetting. As during June, the lack of circulation adjustments outside Asia appears to play an
396 important role in determining magnitude and sign of the aerosol response: the marked anomalous anticyclone over the
397 subtropical western Pacific in the free-running simulations contributes to the strong southerly moisture advection toward
398 southern and eastern China, and thus to the generation of the precipitation increase (Fig. 3g and 3f). These features are of
399 very weak magnitude in the nudged experiments due to the fixed circulation, leading to prevalently dry conditions over
400 China (as opposed to wet anomalies). This, in turn, contributes to weakening, or even opposing, the anomalous westerly



401 wind across India and Indochina seen in CONT, with these regions now displaying prevalently wet (as opposed to dry)
402 anomalies. These findings highlight a competing role and complex interplay between sub-regional precipitation biases in
403 modulating the response to aerosols.

404 **3.4 Responses in the fixed SST PDRMIP simulations**

405 To ascertain whether the link between climatological biases and aerosol response found above for GA7.1 is common to
406 other models, we analyse the PDRMIP multi-model experiments forced by fixed SST. In particular, models are
407 composited based on the sign of the June precipitation bias over central India (the area 73°–85°E, 20°–28°N,
408 approximately corresponding to the core monsoon region), given its key role in determining the seasonality of the aerosol
409 imprint discussed above. Given the fundamental role of aerosol-cloud interactions in realising the aerosol impact, the
410 CESM1-CAM4 and GISS models are excluded from the analysis as they include only a parameterization of aerosol-
411 radiation interactions (Liu et al., 2018). In fact, these two models display very weak monthly precipitation variations over
412 India and China induced by aerosol changes (not shown). Of the five remaining models, two (i.e., HadGEM3 and IPSL-
413 CM) display precipitation deficit while the other three (i.e., MIROC-SPRINTARS, NorESM1 and CESM1-CAM5)
414 present excessive rainfall over India in June (hereafter DRY and WET ensembles, respectively; Fig. S11). Biases and
415 responses for individual models are shown in Fig. S11.

416
417 DRY features a dipole pattern in the June precipitation bias over Asia with drying across India and most of Indochina and
418 wetting over China, particularly to the south and east (Fig. 6a). Based on the mechanism described above, this pattern
419 provides favourable conditions for aerosol-cloud interactions to come into play over China, leading to anomalous low-
420 tropospheric anticyclonic flow over China (Fig. S12a), thereby reducing precipitation there and shifting it southward (Fig.
421 6c). This leads to compensating precipitation increases over northern India, the BOB and the SCS. Key features of both
422 the bias and response patterns are common, in sign and magnitude, to both HadGEM3 and IPSL-CM (Fig. S11), and
423 overall bear marked similarity to those in HadGEM3-GA7.1 (Fig. 3). One notable difference compared to HadGEM3-
424 GA7.1 is that DRY shows an evident meridional land-ocean contrast in the precipitation distribution over the western
425 Pacific, with the wetting predominantly confined to the ocean and drier Indochina and southeastern China. This feature
426 is recognizable in both HadGEM3 and IPSL-CM, with the former model close to the one employed in this study, which
427 suggests the shift to be related to the differing prescribed SST patterns.

428
429 In order to account for model differences and to more clearly highlight the spatio-temporal changes between early and
430 late summer, Fig. 6b and 6f show incremental variations (i.e., September minus June differences) rather than absolute
431 anomalies. The DRY bias features a relative precipitation excess over India, the northern BOB, and most of Indochina,



432 and a deficit over eastern China. Correspondingly, the aerosol-induced response shows easterly flow (Fig. S12b) and
433 widespread decreased precipitation across the Indian subcontinent in September with respect to June (Fig. 6d) and,
434 associated with an anticyclonic anomalous flow over the SCS (Fig. S12b), contributing to precipitation increases over
435 southern and eastern China. There is again marked similarity between these patterns and those for the HadGEM3-GA7.1.
436 As noted for the June response, there is a strong land-ocean contrast in the WET precipitation distribution over the East
437 Asian sector.

438
439 Turning to the analysis of the WET ensemble, the June bias features precipitation excess over most of India and central
440 and northern China, while deficient precipitation is seen over eastern and southern China (Fig. 6e). This pattern, with
441 opposite anomalies over India and reversed meridional dipole over China compared to DRY, is conducive to strong
442 aerosol-cloud interactions over India and relatively weaker signals over eastern China (compared to DRY). As a result,
443 the WET response displays northeasterly flow and widespread drying over India and a cyclonic anomaly over the tropical
444 western Pacific leading to dry northeasterlies over central and eastern China and wet anomalies over the SCS (Fig. 6g and
445 S12c). The June-to-September incremental bias features an approximately opposite pattern to that in June, and so does
446 the precipitation response (Fig. 6f and 6h). Overall, the reversed polarity of bias and responses in WET compared to DRY
447 and the consistency of the key features of the patterns among the individual models further corroborate the robustness of
448 the physical mechanism proposed above.

449 3.5 Responses in coupled simulations

450 One may wonder whether the findings above, based on the analysis of atmospheric-only models, still hold in fully coupled
451 models and how much they are modulated by including two-way air-sea interactions. First, we analyse the PDRMIP
452 coupled model experiments. For consistency with the analysis of the fixed SST experiments, as well as to include the
453 contribution of air-sea coupling but not the full long-term response of the ocean, which presumably has not adjusted to
454 the time-varying emissions in the transient experiments, the analysis was restricted to the first 6–15 years of the
455 simulations. All five chosen models display a dry bias over India in June (Fig. S13) and thus Fig. 7 only shows the DRY
456 multi-model ensemble. In common with the experiments investigated above, the June bias features dry anomalies over
457 South Asia and wet anomalies over southern China (Fig. 7a). A noticeable difference compared to HadGEM3-GC2 is the
458 large-scale drying over the SCS and western subtropical Pacific, showing a meridional dipole. This dipole is obvious in
459 most individual models except for HadGEM3 (mostly zonal; Fig. S13). In September, the dry bias over the Indian sector
460 and western subtropical Pacific undergoes a marked reduction, while the wetting over China is restricted to the central
461 regions.



462 To further examine the robustness of the results, we also analyse the HadGEM3-GC2 coupled transient simulations, which
463 are a close counterpart to the simulations discussed in Section 3.1. The bias pattern and magnitude in the coupled
464 experiment bear a close similarity to that of the HadGEM3-GA7.1 model during both June and September (Fig. 8a and
465 8b), including the dipole between India and central-southeastern China and its sign reversal between early and late
466 summer. This suggests the underlying cause to be rooted in the atmospheric component (Bollasina and Nigam, 2009;
467 Song and Zhou, 2014). The June precipitation response features widespread wetting over India and a large southwest to
468 northeast oriented dipole over China, with excess precipitation over the western Pacific and drying from northern
469 Indochina across southeastern China to Japan (Fig. 8b). These two main features, of comparable magnitude, are also
470 evident in Fig. 3. The main difference is that the dipole is slightly shifted southeastward in the coupled model, associated
471 with the anticyclonic circulation extending over the SCS due to aerosol-induced oceanic cooling (not shown), with
472 consequent opposite sign precipitation anomalies over southeastern China. Also, in agreement with the atmospheric-only
473 simulations, the September response shows extensive drying across South Asia and wetting over southeastern China. As
474 in June, oceanic coupling appears to lead to some differences over southeastern China and the SCS, where the precipitation
475 anomalies, modulated by the slower oceanic response, are slightly shifted over the ocean compared to the uncoupled
476 simulations. These reversed bias patterns are similar to those noted for the PDRMIP coupled model experiments albeit
477 with a different orientation. Correspondingly, both the June and September responses follow the shapes of bias patterns
478 as those shown in Fig. 7, further attesting to the pervasiveness and consistency of the link between bias and aerosol
479 response across different models.

480 **4 Conclusions**

481 While numerous studies have emphasised the key role of anthropogenic aerosols in driving seasonal-mean changes in the
482 Asian monsoon, only very few of them have focused on the aerosol impact at sub-seasonal (e.g., monthly) time scale (e.g.,
483 Lau and Kim, 2006; Bollasina et al., 2013; Fang et al., 2023). Yet, the onset and withdrawal phases of the monsoon are
484 of key importance for the regional economy and water resources as they herald the arrival and demise of the monsoon
485 rains, which provide up to 75% of the total annual rainfall for large areas of Asia. For example, a delayed monsoon onset
486 as well as an early monsoon retreat, or long-term trends in their timings induced by anthropogenic aerosols, can lead to
487 severe consequences for the region. Equally important, inter-model discrepancies in the simulated aerosol-induced
488 monsoon changes at sub-seasonal scale may help to explain the diversity of the seasonal-mean responses.

489
490 Based on the analysis of several climate models and aerosol forcing experiments, we find the sub-seasonal variability of
491 the Asian summer monsoon response to regional anthropogenic aerosol changes to be significantly affected by the spatial
492 pattern and seasonality of the model bias across Asia. The aerosol impact on monsoon precipitation and circulation is



493 strongly influenced by the model ability to simulate the spatial distribution and temporal variability of the climatological
494 monsoon clouds and precipitation, as well as the underlying atmospheric dynamical action centres. These critically
495 modulate the magnitude and efficacy of aerosol-cloud-precipitation interactions, which are the predominant driver of the
496 total aerosol response (e.g., Li et al., 2018; Dong et al., 2021). The amount of available water vapour in the model baseline
497 climatological state exerts a strong control on the extent to which aerosols can interact with clouds and precipitation
498 processes (i.e., via reduced cloud effective radius) and thus modulate the aerosol-induced monsoon response. This
499 involves a strong interplay between South and East Asia and their relative predominance in driving the overall monsoon
500 response, with a striking contrast between the early and late summer aerosol-driven changes ascribable to the seasonal
501 evolution of the biases between the two regions. Our results and proposed mechanism, firstly based on a detailed analysis
502 of atmospheric-only experiments with the HadGEM3-GA7.1 model, are corroborated by the analysis of other atmospheric
503 and coupled models for which sensitivity experiments to Asian aerosol changes are also available.

504
505 In summary, during the onset month (June), models that feature a dry bias over India also display corresponding wet
506 anomalies over eastern China. As the monsoon season progresses and approaches the end (September), the absolute bias
507 decreases, or even reverses, such that incremental changes show wetter conditions over India and drier over eastern China
508 compared to June. Similar variations, but of opposite sign, occur for the models that display a wet June bias over India
509 (and corresponding deficient rainfall over China). These patterns and their sub-seasonal evolution, together with the
510 corresponding atmospheric circulation anomalies, indicate the existence of a strong internal coupling between the South
511 and East Asian monsoon systems, whereby the two components fluctuate and oppose each other at short (monthly or
512 below) time scales. As a result, the aerosol influence on the monsoon, driven by the magnitude of aerosol-cloud
513 interactions, also features a dipole and oscillating pattern between South and East Asia, with the key driving region
514 varying during the season and depending on the evolution of the model climatological state. For example, while the direct
515 aerosol imprint is predominant over East Asia in early summer, it is dominating over South Asia towards the end of the
516 season in the DRY composites. The continental-scale aerosol response, particularly the inter-monsoon interaction,
517 involves an ensuing large-scale atmospheric circulation response, which is pivotal to extending the aerosol impact
518 downstream of the dominating aerosol-forcing region by modulation of the associated moisture transport towards the rest
519 of the domain. The analysis of the nudged experiments further supports the crucial role of non-regional atmospheric
520 circulation adjustments: while keeping the circulation outside Asia close to observations reduces the model bias over Asia,
521 the lack of adjustments under varying Asian aerosol emissions dampens and modifies the pattern and evolution of the
522 regional precipitation response, leading to unrealistic changes (e.g., seasonal mean wetting over South Asia). This
523 suggests that climatological large-scale circulation features, such as the western Pacific subtropical high and the
524 Mascarene high over the southern Indian Ocean, are not only modulated by aerosol forcing over Asia but are also active
525 contributors to generating the aerosol impact itself over Asia.



526

527 The consistency of our findings across different models suggests that the mechanism is robust with respect to the specific
528 model structure and physics, including details of the aerosol module, as long as aerosol-cloud interactions are
529 parameterized. Biases and responses are markedly similar between atmosphere-only and coupled models over land (e.g.,
530 South and East Asia), where the largest aerosol loading is also located and thus the largest forcing is exerted via aerosol-
531 cloud-precipitation interactions. Response patterns between uncoupled and coupled models differ in both magnitude and
532 sign over the surrounding oceanic regions. However, the coupled model response pattern displays an overall minor
533 sensitivity to changes in the averaging period (see Fig. S14 and Fig. 7), with the key anomalies, particularly over land,
534 appearing already in the first decades of the simulation. This indicates that, while air-sea interactions contribute to
535 realising the aerosol impact, the full oceanic response plays a secondary role compared to the predominant action of the
536 atmospheric circulation (Soden and Chung, 2017). This topic, and particularly the analysis of the time scales required to
537 set-up the equilibrium response, has been mostly overlooked in literature, which often compared the fast to the slow
538 response, the latter taken after 50 or more simulated years (e.g., Samset et al., 2016).

539

540 One important implication of the link between model climatological bias and response pattern found here is the possibility
541 of better understanding and constraining the diversity and inconsistencies of model responses to aerosol changes over
542 Asia in historical and future projections by accounting for model deficiencies in simulating the climatological monsoon
543 seasonal cycle compared to observations. This will help in further narrowing the uncertainties associated with aerosol-
544 cloud interactions, given their predominant role in driving the monsoon changes. For example, the clear contrast in the
545 monthly response to aerosols between the PDRMIP DRY and WET composites calls for caution in the interpretation of
546 the aerosol-induced signal without proper consideration of the model baseline performance. This will translate into more
547 robust assessments of sub-regional scale monsoon variations. In fact, despite an overall similarity in the seasonal mean
548 monsoon responses between the DRY and WET ensembles, it is interesting to notice that the difference pattern in
549 precipitation (e.g., DRY minus WET) bears a striking similarity to the observational pattern (Fig. S15 and Fig. S1).

550

551 Differences exist between the observed monsoon changes during the recent decades shown above (Jin and Wang, 2017;
552 Monerie et al., 2022) and those over a longer period (e.g., late 20th century) documented in previous literature and
553 attributed to the dominating regional aerosol forcing, and sulfate aerosols in particular. For example, the increase in
554 anthropogenic aerosol emissions over Asia in the second half of the 20th century has been found to play a key role in
555 driving the observed southern flood-northern dry rainfall dipole over East Asia (Gong and Ho, 2002; Song et al., 2014b;
556 Dong et al., 2016), as well as the South Asian monsoon decline (Gu et al., 2006; Bartlett et al., 2018; Dong et al., 2016;
557 Jiang et al., 2013). A combination of factors, including internal climate variability, may have contributed to these recent
558 trends (Huang et al., 2020b; Monerie et al., 2022) or to set background (oceanic) conditions on top of which aerosols



559 acted (Lin et al., 2016b). While the findings of our study on the possible role of aerosols are necessarily not conclusive,
560 the model bias is found to be equally important to explain model discrepancies. A careful examination of these biases
561 could help reconcile the generally poor performance of state-of-the-art climate models in reproducing recently observed
562 trends (Huang et al., 2020b; Monerie et al., 2022).

563
564 It is also worth emphasizing that the analysis carried out above focuses on the impact of sulfate aerosol emission changes,
565 either because of their marked dominance over other aerosol components (e.g., BC and OC) in the historical period
566 investigated with the HadGEM3-GA7.1 and HadGEM3-GC2 experiments or because of experimental design in the
567 PDRMIP simulations. While sulfate aerosol emissions underwent the largest changes across Asia throughout the historical
568 period (e.g., Lund et al., 2019), the imprint of BC aerosols, although of comparatively weaker magnitude (e.g., Liu et al.,
569 2018; Westervelt et al., 2018), needs also to be accounted to interpret the full extent of the simulated monsoon response
570 to historical aerosol changes and its inter-model inconsistencies given, for example, their different physical mechanisms
571 and responses of opposite sign compared to those due to sulfate aerosols (e.g., Xie et al., 2020).

572
573 The competition between South Asia and East Asia in generating the continental-scale monsoon response and the
574 underpinning modulation by the bias pattern is very relevant in the context of interpreting near-future monsoon projections
575 and related uncertainties, including for regional attribution studies, given the present-day and near-future dipole pattern
576 of emission changes between the two regions (Lund et al., 2019; Samset et al., 2019). For example, it is conceivable to
577 expect that a reduced model bias over South Asia, particularly in early summer, would further promote the importance of
578 Indian aerosol emissions compared to those over China. This also highlights the potential key role of non-local aerosols
579 in driving the simulated response across Asia, which is again crucial in interpreting future projections.

580
581 We acknowledge some limitations of this study. Only a few models are available in each of the DRY and WET composites
582 as aerosol-cloud interactions are not parameterised in some of the PDRMIP models. There are also inter-model differences
583 in the aerosol setups (i.e., prescribed concentrations or emissions) the implications of which are difficult to ascertain given
584 the limited model sample. Including more models and conducting coordinated perturbed aerosol experiments to Asian
585 aerosols would further increase the robustness of our study. It would be interesting to extend this analysis to a longer
586 period and examine, for example, the 20th-century monsoon changes. Internal climate variability may also play an
587 important role and partially mask or offset externally-driven changes, especially given the relatively short time period
588 examined here.

589
590 **Data availability.** The GPCP and CMAP observational datasets are obtained from
591 <https://www.esrl.noaa.gov/psd/data/grid-ded/data.gpcp.html> and <https://psl.noaa.gov/data/gridded/data.cmap.html>,



592 respectively. The ERA-I reanalysis used for nudging can be accessed from
593 <https://www.ecmwf.int/en/forecasts/datasets/reanalysis-datasets/era-interim> (Dee et al., 2011). The ERA5 reanalysis is
594 provided by the European Center for Medium-Range Weather Forecasts
595 (<https://www.ecmwf.int/en/forecasts/dataset/ecmwf-reanalysis-v5>) (Hersbach et al., 2020). The PDRMIP data can be
596 accessed through the World Data Center
597 for Climate (WDCC) data server at https://doi.org/10.26050/WDCC/PDRMIP_2012-2021 (Andrews et al., 2021). The
598 model simulation output is available from the corresponding author on reasonable request.

599

600 **Author contribution.** MAB and ZL designed the study. ZL ran the model simulations. ZL and MAB carried out the
601 analysis, visualized the results and discussed the results. All authors edited the paper.

602

603 **Competing interests.** At least one of the (co-)authors is a member of the editorial board of Atmospheric Chemistry and
604 Physics. The authors also have no other competing interests to declare.

605

606 **Acknowledgements.** ZL is supported by the start-up funding (G0101000155) of the Hong Kong University of Science
607 and Technology (Guangzhou). MB is supported by the Natural Environment Research Council (grant no. NE/N006038/1).
608 MB and LW acknowledge support from the Research Council of Norway (grant no. 324182; CATHY). ZL, MB, and LW
609 were supported by the UK-China Research and Innovation Partnership Fund through the Met Office Climate Science for
610 Service Partnership (CSSP) China as part of the Newton Fund. We acknowledge the use of ARCHER, the UK HPC, and
611 of the JASMIN super-data-cluster.

612 References

613 Adler, R. F., Huffman, G. J., Chang, A., Ferraro, R., Xie, P. P., Janowiak, J., Rudolf, B., Schneider, U., Curtis, S., Bolvin,
614 D., Gruber, A., Susskind, J., Arkin, P., and Nelkin, E.: The version-2 global precipitation climatology project (GPCP)
615 monthly precipitation analysis (1979-present), *Journal of Hydrometeorology*, [https://doi.org/10.1175/1525-7541\(2003\)004<1147:TVGPCP>2.0.CO;2](https://doi.org/10.1175/1525-7541(2003)004<1147:TVGPCP>2.0.CO;2), 2003.

617 Albrecht, B. A.: Aerosols, cloud microphysics, and fractional cloudiness, *Science*,
618 <https://doi.org/10.1126/science.245.4923.1227>, 1989.

619 An, Z., Colman, S. M., Zhou, W., Li, X., Brown, E. T., Jull, A. J. T., Cai, Y., Huang, Y., Lu, X., Chang, H., Song, Y.,
620 Sun, Y., Xu, H., Liu, W., Jin, Z., Liu, X., Cheng, P., Liu, Y., Ai, L., Li, X., Liu, X., Yan, L., Shi, Z., Wang, X., Wu,
621 F., Qiang, X., Dong, J., Lu, F., and Xu, X.: Interplay between the Westerlies and Asian monsoon recorded in Lake
622 Qinghai sediments since 32 ka, *Scientific Reports*, <https://doi.org/10.1038/srep00619>, 2012.



- 623 Andrews, T., Boucher, O., Fläschner, D., Kasoar, M., Kharin, V., Kirkevåg, A., Lamarque, J.-F., Myhre, G., Mülsenstädt,
624 J., Olivieri, D. J. L., Samset, B., Sandstad, M., Shawki, D., Shindell, D., Stier, P., Takemura, T., Voulgarakis, A., and
625 Watson-Parris, D.: Precipitation Driver Response Model Intercomparison Project data sets 2013–2021, World Data
626 Center for Climate (WDCC) at DKRZ, https://doi.org/10.26050/WDCC/PDRMIP_2012-2021, 2021.
- 627 Andrews, T. and Forster, P. M.: Energy budget constraints on historical radiative forcing, *Nature Climate Change*, 10,
628 313–316, <https://doi.org/10.1038/s41558-020-0696-1>, 2020.
- 629 Bartlett, R. E., Bollasina, M. A., Booth, B. B. B., Dunstone, N. J., Marengo, F., Messori, G., and Bernie, D. J.: Do
630 differences in future sulfate emission pathways matter for near-term climate? A case study for the Asian monsoon,
631 *Climate Dynamics*, <https://doi.org/10.1007/s00382-017-3726-6>, 2018.
- 632 Bastin, S., Drobinski, P., Chiriaco, M., Bock, O., Roehrig, R., Gallardo, C., Conte, D., Domínguez Alonso, M., Li, L.,
633 Lionello, P., and Parracho, A. C.: Impact of humidity biases on light precipitation occurrence: Observations versus
634 simulations, *Atmospheric Chemistry and Physics*, <https://doi.org/10.5194/acp-19-1471-2019>, 2019.
- 635 Bellouin, N., Mann, G. W., Woodhouse, M. T., Johnson, C., Carslaw, K. S., and Dalvi, M.: Impact of the modal aerosol
636 scheme GLOMAP-mode on aerosol forcing in the hadley centre global environmental model, *Atmospheric Chemistry
637 and Physics*, <https://doi.org/10.5194/acp-13-3027-2013>, 2013.
- 638 Bollasina, M. and Nigam, S.: Indian Ocean SST, evaporation, and precipitation during the South Asian summer monsoon
639 in IPCC-AR4 coupled simulations, *Climate Dynamics*, <https://doi.org/10.1007/s00382-008-0477-4>, 2009.
- 640 Bollasina, M. A., Ming, Y., and Ramaswamy, V.: Anthropogenic aerosols and the weakening of the south asian summer
641 monsoon, *Science*, <https://doi.org/10.1126/science.1204994>, 2011.
- 642 Bollasina, M. A., Ming, Y., and Ramaswamy, V.: Earlier onset of the Indian monsoon in the late twentieth century: The
643 role of anthropogenic aerosols, *Geophysical Research Letters*, <https://doi.org/10.1002/grl.50719>, 2013.
- 644 Bollasina, M. A., Ming, Y., Ramaswamy, V., Schwarzkopf, M. D., and Naik, V.: Contribution of local and remote
645 anthropogenic aerosols to the twentieth century weakening of the South Asian Monsoon, *Geophysical Research
646 Letters*, <https://doi.org/10.1002/2013GL058183>, 2014.
- 647 Boucher, O., Randall, D., Artaxo, P., Bretherton, C., Feingold, G., Forster, P., Kerminen, V.-M., Kondo, Y., Liao, H.,
648 Lohmann, U., Rasch, P., Satheesh, S. K., Sherwood, S., Stevens, B., and Zhang, X. Y.: IPCC, 2013: Clouds and
649 Aerosols., in: *Climate Change 2013: The Physical Science Basis. Contribution of Working Group I to the Fifth
650 Assessment Report of the Intergovernmental Panel on Climate Change*,
651 <https://doi.org/10.1017/CBO9781107415324.016>, 2013.
- 652 Cao, J., Wang, B., Wang, B., Zhao, H., Wang, C., and Han, Y.: Sources of the Intermodel Spread in Projected Global
653 Monsoon Hydrological Sensitivity, *Geophysical Research Letters*, <https://doi.org/10.1029/2020GL089560>, 2020.
- 654 Chadwick, R.: Which aspects of CO₂ forcing and SST warming cause most uncertainty in projections of tropical rainfall
655 change over land and ocean?, *Journal of Climate*, <https://doi.org/10.1175/JCLI-D-15-0777.1>, 2016.
- 656 Chen, X., Wu, P., Roberts, M. J., and Zhou, T.: Potential underestimation of future Mei-Yu Rainfall with coarse-resolution
657 climate models, *Journal of Climate*, 31, 6711–6727, <https://doi.org/10.1175/JCLI-D-17-0741.1>, 2018.



- 658 Christidis, N., Stott, P. A., Scaife, A. A., Arribas, A., Jones, G. S., Copsey, D., Knight, J. R., and Tennant, W. J.: A new
659 HADGEM3-a-based system for attribution of weather- and climate-related extreme events, *Journal of Climate*,
660 <https://doi.org/10.1175/JCLI-D-12-00169.1>, 2013.
- 661 Chung, C. E. and Ramanathan, V.: Weakening of north Indian SST gradients and the monsoon rainfall in India and the
662 Sahel, *Journal of Climate*, <https://doi.org/10.1175/JCLI3820.1>, 2006.
- 663 Cowan, T. and Cai, W.: The impact of Asian and non-Asian anthropogenic aerosols on 20th century Asian summer
664 monsoon, *Geophysical Research Letters*, <https://doi.org/10.1029/2011GL047268>, 2011.
- 665 Dai, L., Cheng, T. F., and Lu, M.: Anthropogenic warming disrupts intraseasonal monsoon stages and brings dry-get-
666 wetter climate in future East Asia, *npj Climate and Atmospheric Science*, [https://doi.org/10.1038/s41612-022-00235-](https://doi.org/10.1038/s41612-022-00235-9)
667 9, 2022.
- 668 Dee, D. P., Uppala, S. M., Simmons, A. J., Berrisford, P., Poli, P., Kobayashi, S., Andrae, U., Balmaseda, M. A., Balsamo,
669 G., Bauer, P., Bechtold, P., Beljaars, A. C. M., van de Berg, L., Bidlot, J., Bormann, N., Delsol, C., Dragani, R.,
670 Fuentes, M., Geer, A. J., Haimberger, L., Healy, S. B., Hersbach, H., Hólm, E. V., Isaksen, I., Kållberg, P., Köhler,
671 M., Matricardi, M., McNally, A. P., Monge-Sanz, B. M., Morcrette, J. J., Park, B. K., Peubey, C., de Rosnay, P.,
672 Tavolato, C., Thépaut, J. N., and Vitart, F.: The ERA-Interim reanalysis: Configuration and performance of the data
673 assimilation system, *Quarterly Journal of the Royal Meteorological Society*, <https://doi.org/10.1002/qj.828>, 2011.
- 674 Deser, C., Phillips, A., Bourdette, V., and Teng, H.: Uncertainty in climate change projections: The role of internal
675 variability, *Climate Dynamics*, <https://doi.org/10.1007/s00382-010-0977-x>, 2012.
- 676 Dong, B., Sutton, R. T., Highwood, E. J., and Wilcox, L. J.: Preferred response of the East Asian summer monsoon to
677 local and non-local anthropogenic sulphur dioxide emissions, *Climate Dynamics*, [https://doi.org/10.1007/s00382-015-](https://doi.org/10.1007/s00382-015-2671-5)
678 2671-5, 2016.
- 679 Efron, B., & Tibshirani, R. J. (1993). An introduction to the bootstrap, *Monographs on Statistics and Applied Probability*,
680 (Vol. 57, p. 436). London: Chapman and Hall. <https://doi.org/10.1111/1467-9639.00050>
- 681 Fang, C., Haywood, J. M., Liang, J., Johnson, B. T., Chen, Y., and Zhu, B.: Impacts of reducing scattering and absorbing
682 aerosols on the temporal extent and intensity of South Asian summer monsoon and East Asian summer monsoon,
683 *Atmospheric Chemistry and Physics*, 23, 8341–8368, <https://doi.org/10.5194/ACP-23-8341-2023>, 2023.
- 684 Fläschner, D., Mauritsen, T., and Stevens, B.: Understanding the intermodel spread in global-mean hydrological
685 sensitivity, *Journal of Climate*, <https://doi.org/10.1175/JCLI-D-15-0351.1>, 2016.
- 686 Ganguly, D., Rasch, P. J., Wang, H., and Yoon, J. H.: Fast and slow responses of the South Asian monsoon system to
687 anthropogenic aerosols, *Geophysical Research Letters*, <https://doi.org/10.1029/2012GL053043>, 2012.
- 688 Gong, D.-Y. and Ho, C.-H.: Shift in the summer rainfall over the Yangtze River valley in the late 1970s, *Geophysical*
689 *Research Letters*, <https://doi.org/10.1029/2001gl014523>, 2002.
- 690 Gu, Y., Liou, K. N., Xue, Y., Mechoso, C. R., Li, W., and Luo, Y.: Climatic effects of different aerosol types in China
691 simulated by the UCLA general circulation model, *Journal of Geophysical Research Atmospheres*,
692 <https://doi.org/10.1029/2005JD006312>, 2006.



- 693 Guilbert, M., Terray, P., and Mignot, J.: Intermodel spread of historical Indian monsoon rainfall change in CMIP6: The
694 role of the tropical Pacific mean-state, *Journal of Climate*, 1, 1–42, <https://doi.org/10.1175/JCLI-D-22-0585.1>, 2023.
- 695 Guo, L., Highwood, E. J., Shaffrey, L. C., and Turner, A. G.: The effect of regional changes in anthropogenic aerosols on
696 rainfall of the East Asian Summer Monsoon, *Atmospheric Chemistry and Physics*, [https://doi.org/10.5194/acp-13-](https://doi.org/10.5194/acp-13-1521-2013)
697 1521-2013, 2013.
- 698 Guo, L., Turner, A. G., and Highwood, E. J.: Impacts of 20th century aerosol emissions on the South Asian monsoon in
699 the CMIP5 models, *Atmospheric Chemistry and Physics*, <https://doi.org/10.5194/acp-15-6367-2015>, 2015.
- 700 Han, Y., Zhang, M. Z., Xu, Z., and Guo, W.: Assessing the performance of 33 CMIP6 models in simulating the large-
701 scale environmental fields of tropical cyclones, *Climate Dynamics*, <https://doi.org/10.1007/s00382-021-05986-4>,
702 2022.
- 703 He, J. and Soden, B. J.: The impact of SST biases on projections of anthropogenic climate change: A greater role for
704 atmosphere-only models?, *Geophysical Research Letters*, <https://doi.org/10.1002/2016GL069803>, 2016.
- 705 He, L., Zhou, T., and Chen, X.: South Asian summer rainfall from CMIP3 to CMIP6 models: biases and improvements,
706 *Climate Dynamics*, <https://doi.org/10.1007/s00382-022-06542-4>, 2022.
- 707 Herbert, R., Wilcox, L. J., Joshi, M., Highwood, E., and Frame, D.: Nonlinear response of Asian summer monsoon
708 precipitation to emission reductions in South and East Asia, *Environmental Research Letters*,
709 <https://doi.org/10.1088/1748-9326/ac3b19>, 2022.
- 710 Hersbach, H., Bell, B., Berrisford, P., Hirahara, S., Horányi, A., Muñoz-Sabater, J., Nicolas, J., Peubey, C., Radu, R.,
711 Schepers, D., Simmons, A., Soci, C., Abdalla, S., Abellan, X., Balsamo, G., Bechtold, P., Biavati, G., Bidlot, J.,
712 Bonavita, M., De Chiara, G., Dahlgren, P., Dee, D., Diamantakis, M., Dragani, R., Flemming, J., Forbes, R., Fuentes,
713 M., Geer, A., Haimberger, L., Healy, S., Hogan, R. J., Hólm, E., Janisková, M., Keeley, S., Laloyaux, P., Lopez, P.,
714 Lupu, C., Radnoti, G., de Rosnay, P., Rozum, I., Vamborg, F., Villaume, S., and Thépaut, J. N.: The ERA5 global
715 reanalysis, *Quarterly Journal of the Royal Meteorological Society*, 146, 1999–2049, <https://doi.org/10.1002/qj.3803>,
716 2020.
- 717 Hoesly, R. M., Smith, S. J., Feng, L., Klimont, Z., Janssens-Maenhout, G., Pitkanen, T., Seibert, J. J., Vu, L., Andres, R.
718 J., Bolt, R. M., Bond, T. C., Dawidowski, L., Kholod, N., Kurokawa, J. I., Li, M., Liu, L., Lu, Z., Moura, M. C. P.,
719 O'Rourke, P. R., and Zhang, Q.: Historical (1750-2014) anthropogenic emissions of reactive gases and aerosols from
720 the Community Emissions Data System (CEDS), *Geoscientific Model Development*, [https://doi.org/10.5194/gmd-11-](https://doi.org/10.5194/gmd-11-369-2018)
721 369-2018, 2018.
- 722 Huang, X., Zhou, T., Dai, A., Li, H., Li, C., Chen, X., Lu, J., von Storch, J. S., and Wu, B.: South Asian summer monsoon
723 projections constrained by the interdecadal Pacific oscillation, *Science Advances*,
724 <https://doi.org/10.1126/sciadv.aay6546>, 2020a.
- 725 Huang, X., Zhou, T., Turner, A., Dai, A., Chen, X., Clark, R., Jiang, J., Man, W., Murphy, J., Rostron, J., Wu, B., Zhang,
726 L., Zhang, W., and Zou, L.: The recent decline and recovery of Indian summer monsoon rainfall: Relative roles of
727 external forcing and internal variability, *Journal of Climate*, <https://doi.org/10.1175/JCLI-D-19-0833.1>, 2020b.



- 728 Jiang, D., Hu, D., Tian, Z., and Lang, X.: Differences between CMIP6 and CMIP5 Models in Simulating Climate over
729 China and the East Asian Monsoon, *Advances in Atmospheric Sciences*, <https://doi.org/10.1007/s00376-020-2034-y>,
730 2020.
- 731 Jiang, Y., Liu, X., Yang, X. Q., and Wang, M.: A numerical study of the effect of different aerosol types on East Asian
732 summer clouds and precipitation, *Atmospheric Environment*, 70, 51–63,
733 <https://doi.org/10.1016/j.atmosenv.2012.12.039>, 2013.
- 734 Jin, Q. and Wang, C.: A revival of Indian summer monsoon rainfall since 2002, *Nature Climate Change*,
735 <https://doi.org/10.1038/NCLIMATE3348>, 2017.
- 736 John, V. O. and Soden, B. J.: Temperature and humidity biases in global climate models and their impact on climate
737 feedbacks, *Geophysical Research Letters*, <https://doi.org/10.1029/2007GL030429>, 2007.
- 738 Keane, R. J., Williams, K. D., Stirling, A. J., Martin, G. M., Birch, C. E., and Parker, D. J.: Fast biases in monsoon rainfall
739 over southern and central India in the Met Office unified model, *Journal of Climate*, <https://doi.org/10.1175/JCLI-D-18-0650.1>, 2019.
- 741 Kooperman, G. J., Pritchard, M. S., Ghan, S. J., Wang, M., Somerville, R. C. J., and Russell, L. M.: Constraining the
742 influence of natural variability to improve estimates of global aerosol indirect effects in a nudged version of the
743 Community Atmosphere Model 5, *Journal of Geophysical Research Atmospheres*,
744 <https://doi.org/10.1029/2012JD018588>, 2012.
- 745 Krinner, G. and Flanner, M. G.: Striking stationarity of large-scale climate model bias patterns under strong climate
746 change, *Proceedings of the National Academy of Sciences of the United States of America*,
747 <https://doi.org/10.1073/pnas.1807912115>, 2018.
- 748 Lau, K. M. and Kim, K. M.: Observational relationships between aerosol and Asian monsoon rainfall, and circulation,
749 *Geophysical Research Letters*, <https://doi.org/10.1029/2006GL027546>, 2006.
- 750 Lau, W. K. M. and Kim, K. M.: Fingerprinting the impacts of aerosols on long-term trends of the Indian summer monsoon
751 regional rainfall, *Geophysical Research Letters*, <https://doi.org/10.1029/2010GL043255>, 2010.
- 752 Li, X., Ting, M., and Lee, D. E.: Fast Adjustments of the Asian Summer Monsoon to Anthropogenic Aerosols,
753 *Geophysical Research Letters*, <https://doi.org/10.1002/2017GL076667>, 2018.
- 754 Li, X., Ting, M., You, Y., Lee, D. E., Westervelt, D. M., and Ming, Y.: South Asian Summer Monsoon Response to
755 Aerosol-Forced Sea Surface Temperatures, *Geophysical Research Letters*, <https://doi.org/10.1029/2019GL085329>,
756 2020.
- 757 Lin, J., Tong, D., Davis, S., Ni, R., Tan, X., Pan, D., Zhao, H., Lu, Z., Streets, D., Feng, T., Zhang, Q., Yan, Y., Hu, Y.,
758 Li, J., Liu, Z., Jiang, X., Geng, G., He, K., Huang, Y., and Guan, D.: Global climate forcing of aerosols embodied in
759 international trade, *Nature Geoscience*, <https://doi.org/10.1038/ngeo2798>, 2016a.
- 760 Lin, R., Zhu, J., and Zheng, F.: Decadal shifts of East Asian summer monsoon in a climate model free of explicit GHGs
761 and aerosols, *Scientific Reports*, <https://doi.org/10.1038/srep38546>, 2016b.



- 762 Liu, C., Yang, Y., Wang, H., Ren, L., Wei, J., Wang, P., and Liao, H.: Influence of Spatial Dipole Pattern in Asian Aerosol
763 Changes on East Asian Summer Monsoon, *Journal of Climate*, 36, 1575–1585, <https://doi.org/10.1175/JCLI-D-22->
764 0335.1, 2023.
- 765 Liu, L., Shawki, D., Voulgarakis, A., Kasoar, M., Samset, B. H., Myhre, G., Forster, P. M., Hodnebrog, Sillmann, J.,
766 Aalbergsjø, S. G., Boucher, O., Faluvegi, G., Iversen, T., Kirkevåg, A., Lamarque, J. F., Olivieć, D., Richardson, T.,
767 Shindell, D., and Takemura, T.: A PDRMIP Multimodel study on the impacts of regional aerosol forcings on global
768 and regional precipitation, *Journal of Climate*, <https://doi.org/10.1175/JCLI-D-17-0439.1>, 2018.
- 769 Liu, Z., Bollasina, M. A., Wilcox, L. J., Rodríguez, J. M., and Regayre, L. A.: Contrasting the Role of Regional and
770 Remote Circulation in Driving Asian Monsoon Biases in MetUM GA7.1, *Journal of Geophysical Research:*
771 *Atmospheres*, 126, <https://doi.org/10.1029/2020JD034342>, 2021.
- 772 Liu, Z., Lee, S.-S., Nelliikkattil, A. B., Lee, J.-Y., Dai, Lan, Ha, K.-J., Christian, J., and Franzke, L. E.: The East Asian
773 Summer Monsoon Response to Global Warming in a High Resolution Coupled Model: Mean and Extremes, *Asia-*
774 *Pacific Journal of Atmospheric Sciences* 2022, 1–17, <https://doi.org/10.1007/S13143-022-00285-2>, 2022.
- 775 Lund, M. T., Myhre, G., and Samset, B. H.: Anthropogenic aerosol forcing under the Shared Socioeconomic Pathways,
776 *Atmospheric Chemistry and Physics*, <https://doi.org/10.5194/acp-19-13827-2019>, 2019.
- 777 Mann, G. W., Carslaw, K. S., Spracklen, D. V., Ridley, D. A., Manktelow, P. T., Chipperfield, M. P., Pickering, S. J.,
778 and Johnson, C. E.: Description and evaluation of GLOMAP-mode: A modal global aerosol microphysics model for
779 the UKCA composition-climate model, *Geoscientific Model Development*, <https://doi.org/10.5194/gmd-3-519-2010>,
780 2010.
- 781 Matsueda, M. and Palmer, T. N.: Accuracy of climate change predictions using high resolution simulations as surrogates
782 of truth, *Geophysical Research Letters*, <https://doi.org/10.1029/2010GL046618>, 2011.
- 783 Menon, S., Hansen, J., Nazarenko, L., and Luo, Y.: Climate effects of black carbon aerosols in China and India, *Science*,
784 <https://doi.org/10.1126/science.1075159>, 2002a.
- 785 Menon, S., Del Genio, A. D., Koch, D., and Tselioudis, G.: GCM simulations of the aerosol indirect effect: Sensitivity to
786 cloud parameterization and aerosol Burden, *Journal of the Atmospheric Sciences*, <https://doi.org/10.1175/1520->
787 0469(2002)059<0692:gsotai>2.0.co;2, 2002b.
- 788 Monerie, P. A., Wilcox, L. J., and Turner, A. G.: Effects of Anthropogenic Aerosol and Greenhouse Gas Emissions on
789 Northern Hemisphere Monsoon Precipitation: Mechanisms and Uncertainty, *Journal of Climate*,
790 <https://doi.org/10.1175/JCLI-D-21-0412.1>, 2022.
- 791 Myhre, G., Forster, P. M., Samset, B. H., Hodnebrog, Sillmann, J., Aalbergsjø, S. G., Andrews, T., Boucher, O., Faluvegi,
792 G., Fläschner, D., Iversen, T., Kasoar, M., Kharin, V., Kirkevåg, A., Lamarque, J. F., Olivieć, D., Richardson, T. B.,
793 Shindell, D., Shine, K. P., Stjern, C. W., Takemura, T., Voulgarakis, A., and Zwiers, F.: PDRMIP: A precipitation
794 driver and response model intercomparison project-protocol and preliminary results, *Bulletin of the American*
795 *Meteorological Society*, <https://doi.org/10.1175/BAMS-D-16-0019.1>, 2017.
- 796 Park, M. and Lee, S.: Is the Stationary Wave Bias in CMIP5 Simulations Driven by Latent Heating Biases?, *Geophysical*
797 *Research Letters*, <https://doi.org/10.1029/2020GL091678>, 2021.



- 798 Pillai, P. A., Rao, S. A., Srivastava, A., Ramu, D. A., Pradhan, M., and Das, R. S.: Impact of the tropical Pacific SST
799 biases on the simulation and prediction of Indian summer monsoon rainfall in CFSv2, ECMWF-System4, and NMME
800 models, *Climate Dynamics*, <https://doi.org/10.1007/s00382-020-05555-1>, 2021.
- 801 Rajendran, K., Surendran, S., Varghese, S. J., and Sathyanath, A.: Simulation of Indian summer monsoon rainfall,
802 interannual variability and teleconnections: evaluation of CMIP6 models, *Climate Dynamics*,
803 <https://doi.org/10.1007/s00382-021-06027-w>, 2022.
- 804 Samset, B. H., Myhre, G., Forster, P. M., Hodnebrog, Andrews, T., Faluvegi, G., Fläschner, D., Kasoar, M., Kharin, V.,
805 Kirkevåg, A., Lamarque, J. F., Olivié, D., Richardson, T., Shindell, D., Shine, K. P., Takemura, T., and Voulgarakis,
806 A.: Fast and slow precipitation responses to individual climate forcings: A PDRMIP multimodel study, *Geophysical
807 Research Letters*, <https://doi.org/10.1002/2016GL068064>, 2016.
- 808 Samset, B. H., Lund, M. T., Bollasina, M., Myhre, G., and Wilcox, L.: Emerging Asian aerosol patterns, *Nature
809 Geoscience*, <https://doi.org/10.1038/s41561-019-0424-5>, 2019.
- 810 Sato, Y., Goto, D., Michibata, T., Suzuki, K., Takemura, T., Tomita, H., and Nakajima, T.: Aerosol effects on cloud water
811 amounts were successfully simulated by a global cloud-system resolving model, *Nature Communications*,
812 <https://doi.org/10.1038/s41467-018-03379-6>, 2018.
- 813 Seager, R., N. Naik, and G. A. Vecchi, 2010: Thermodynamic and dynamic mechanisms for large-scale changes in the
814 hydrological cycle in response to global warming. *J. Climate*, 23, 4651–4668,
815 <https://doi.org/10.1175/2010JCLI3655.1>.
- 816 Sherman, P., Gao, M., Song, S., Archibald, A. T., Luke Abraham, N., Lamarque, J. F., Shindell, D., Faluvegi, G., and
817 McElroy, M. B.: Sensitivity of modeled Indian monsoon to Chinese and Indian aerosol emissions, *Atmospheric
818 Chemistry and Physics*, <https://doi.org/10.5194/acp-21-3593-2021>, 2021.
- 819 Singh, D., Bollasina, M., Ting, M., and Diffenbaugh, N. S.: Disentangling the influence of local and remote anthropogenic
820 aerosols on South Asian monsoon daily rainfall characteristics, *Climate Dynamics*, <https://doi.org/10.1007/s00382-018-4512-9>, 2019.
- 822 Soden, B. and Chung, E.-S.: The Large-Scale Dynamical Response of Clouds to Aerosol Forcing, *Journal of Climate*, 30,
823 8783–8794, <https://doi.org/10.1175/JCLI-D-17-0050.1>, 2017.
- 824 Song, F. and Zhou, T.: The climatology and interannual variability of east Asian summer monsoon in CMIP5 coupled
825 models: Does air-sea coupling improve the simulations?, *Journal of Climate*, <https://doi.org/10.1175/JCLI-D-14-00396.1>, 2014.
- 827 Song, F., Zhou, T., and Qian, Y.: Responses of East Asian summer monsoon to natural and anthropogenic forcings in the
828 17 latest CMIP5 models, *Geophysical Research Letters*, <https://doi.org/10.1002/2013GL058705>, 2014a.
- 829 Song, F., Zhou, T., and Qian, Y.: Responses of East Asian summer monsoon to natural and anthropogenic forcings in the
830 17 latest CMIP5 models, *Geophysical Research Letters*, <https://doi.org/10.1002/2013GL058705>, 2014b.
- 831 Sperber, K. R., Annamalai, H., Kang, I. S., Kitoh, A., Moise, A., Turner, A., Wang, B., and Zhou, T.: The Asian summer
832 monsoon: An intercomparison of CMIP5 vs. CMIP3 simulations of the late 20th century, *Climate Dynamics*, 41,
833 2711–2744, <https://doi.org/10.1007/s00382-012-1607-6>, 2013.



- 834 Tian, F., Dong, B., Robson, J., and Sutton, R.: Forced decadal changes in the East Asian summer monsoon: the roles of
835 greenhouse gases and anthropogenic aerosols, *Climate Dynamics*, <https://doi.org/10.1007/s00382-018-4105-7>, 2018.
- 836 Tong, M., Zheng, Z., and Fu, Q.: Evaluation of East Asian Meiyu from CMIP6/AMIP simulations, 1, 3,
837 <https://doi.org/10.1007/s00382-022-06218-z>, 2022.
- 838 Twomey, S.: Pollution and the planetary albedo, *Atmospheric Environment* (1967), <https://doi.org/10.1016/0004->
839 6981(74)90004-3, 1974.
- 840 Vidya, P. J., Ravichandran, M., Subeesh, M. P., Chatterjee, S., and Nuncio, M.: Global warming hiatus contributed
841 weakening of the Mascarene High in the Southern Indian Ocean, *Scientific Reports*, <https://doi.org/10.1038/s41598->
842 020-59964-7, 2020.
- 843 Walters, D., Baran, A. J., Boutle, I., Brooks, M., Earnshaw, P., Edwards, J., Furtado, K., Hill, P., Lock, A., Manners, J.,
844 Morcrette, C., Mulcahy, J., Sanchez, C., Smith, C., Stratton, R., Tennant, W., Tomassini, L., Van Weverberg, K.,
845 Vosper, S., Willett, M., Browse, J., Bushell, A., Carslaw, K., Dalvi, M., Essery, R., Gedney, N., Hardiman, S.,
846 Johnson, B., Johnson, C., Jones, A., Jones, C., Mann, G., Milton, S., Rumbold, H., Sellar, A., Ujiie, M., Whittall, M.,
847 Williams, K., and Zerroukat, M.: The Met Office Unified Model Global Atmosphere 7.0/7.1 and JULES Global Land
848 7.0 configurations, *Geoscientific Model Development*, 12, 1909–1963, <https://doi.org/10.5194/gmd-12-1909-2019>,
849 2019.
- 850 Wang, B., Yim, S. Y., Lee, J. Y., Liu, J., and Ha, K. J.: Future change of Asian-Australian monsoon under RCP 4.5
851 anthropogenic warming scenario, *Climate Dynamics*, <https://doi.org/10.1007/s00382-013-1769-x>, 2014.
- 852 Wang, B., Jin, C., and Liu, J.: Understanding Future Change of Global Monsoons Projected by CMIP6 Models, *Journal*
853 *of Climate*, 33, 6471–6489, <https://doi.org/10.1175/JCLI-D-19-0993.1>, 2020.
- 854 Wang, N., Zhang, K., Shen, X., Wang, Y., Li, J., Li, C., Mao, J., Malinka, A., Zhao, C., Russell, L. M., Guo, J., Gross,
855 S., Liu, C., Yang, J., Chen, F., Sijie Chen¹, L. W., Ke, J., Xiao, D., Zhou, Y., Fang, J., and Liu, D.: Dual-field-of-view
856 high-spectral-resolution lidar: Simultaneous profiling of aerosol and water cloud to study aerosol-cloud interaction,
857 *Proceedings of the National Academy of Sciences of the United States of America*,
858 <https://doi.org/10.1073/pnas.2110756119>, 2022.
- 859 Wilcox, L., Dunstone, N., Lewinschal, A., Bollasina, M., Ekman, A., and Highwood, E.: Mechanisms for a remote
860 response to Asian anthropogenic aerosol in boreal winter, *Atmospheric Chemistry and Physics*,
861 <https://doi.org/10.5194/acp-19-9081-2019>, 2019.
- 862 Wilcox, L. J., Dong, B., Sutton, R. T., and Highwood, E. J.: The 2014 hot, dry summer in northeast Asia, *Bulletin of the*
863 *American Meteorological Society*, 96, S105–S110, <https://doi.org/10.1175/BAMS-D-15-00123.1>, 2015.
- 864 Wilcox, L. J., Liu, Z., Samset, B. H., Hawkins, E., Lund, M. T., Nordling, K., Undorf, S., Bollasina, M., Ekman, A. M.
865 L., Krishnan, S., Merikanto, J., and Turner, A. G.: Accelerated increases in global and Asian summer monsoon
866 precipitation from future aerosol reductions, *Atmos. Chem. Phys.*, 20, 11955–11977, <https://doi.org/10.5194/acp-20->
867 11955-2020, 2020.
- 868 Xie, P. and Arkin, P. A.: Global Precipitation: A 17-Year Monthly Analysis Based on Gauge Observations, Satellite
869 Estimates, and Numerical Model Outputs, *Bulletin of the American Meteorological Society*,
870 [https://doi.org/10.1175/1520-0477\(1997\)078<2539:GPAYMA>2.0.CO;2](https://doi.org/10.1175/1520-0477(1997)078<2539:GPAYMA>2.0.CO;2), 1997.



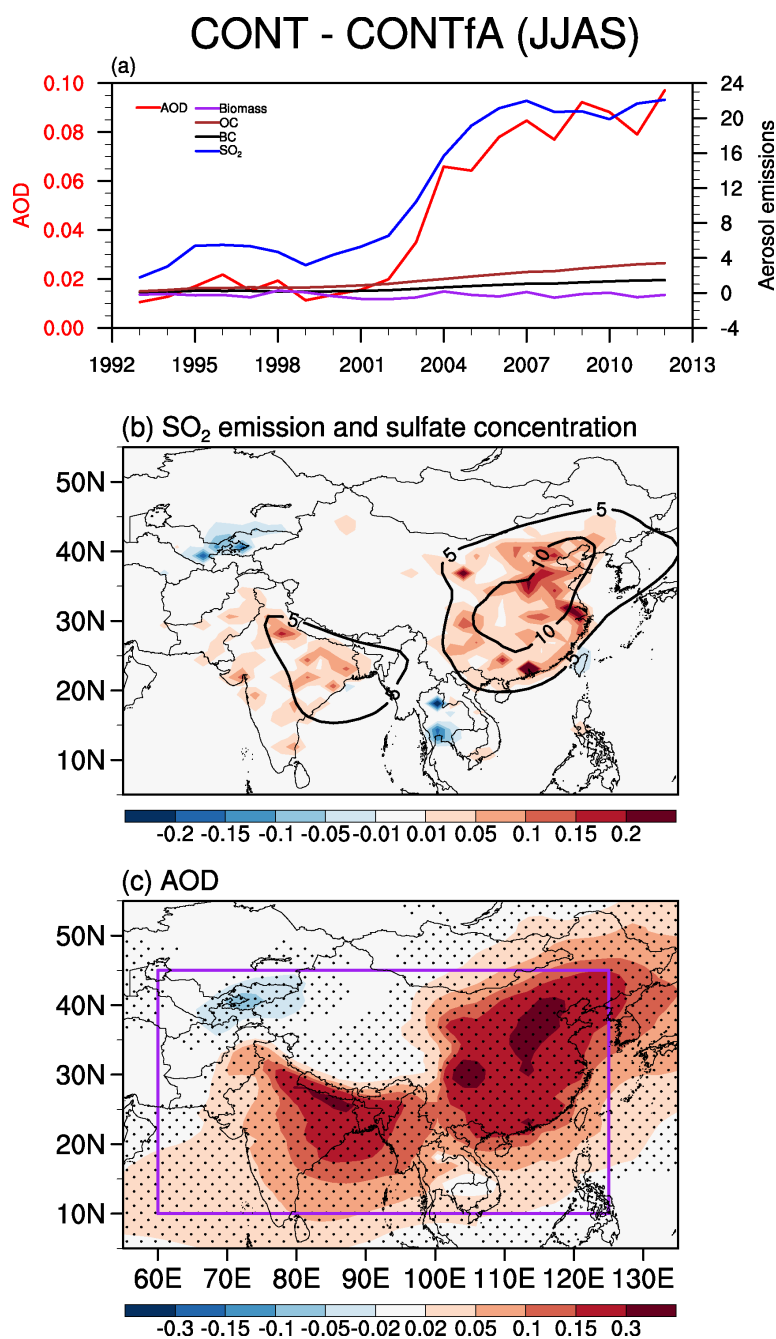
- 871 Xie, X., Myhre, G., Liu, X., Li, X., Shi, Z., Wang, H., Kirkevåg, A., Lamarque, J.-F., Shindell, D., Takemura, T., and
872 Liu, Y.: Distinct responses of Asian summer monsoon to black carbon aerosols and greenhouse gases, *Atmos. Chem.*
873 *Phys.*, 20, 11823–11839, <https://doi.org/10.5194/acp-20-11823-2020>, 2020.
- 874 Yang, B., Zhang, Y., Qian, Y., Song, F., Leung, L. R., Wu, P., Guo, Z., Lu, Y., and Huang, A.: Better monsoon
875 precipitation in coupled climate models due to bias compensation, *npj Climate and Atmospheric Science*,
876 <https://doi.org/10.1038/s41612-019-0100-x>, 2019.
- 877 Yu, S., Li, P., Wang, L., Wang, P., Wang, S., Chang, S., Liu, W., and Alapaty, K.: Anthropogenic aerosols are a potential
878 cause for migration of the summer monsoon rain belt in China, *Proceedings of the National Academy of Sciences of*
879 *the United States of America*, <https://doi.org/10.1073/pnas.1601104113>, 2016.
- 880 Zanis, P., Akritidis, D., Georgoulias, K. A., Allen, J. R., Bauer, E. S., Boucher, O., Cole, J., Johnson, B., Deushi, M.,
881 Michou, M., Mulcahy, J., Nabat, P., Olivié, D., Oshima, N., Sima, A., Schulz, M., Takemura, T., and Tsigaridis, K.:
882 Fast responses on pre-industrial climate from present-day aerosols in a CMIP6 multi-model study, *Atmospheric*
883 *Chemistry and Physics*, <https://doi.org/10.5194/acp-20-8381-2020>, 2020.
- 884 Zha, J., Shen, C., Zhao, D., Feng, J., Xu, Z., Wu, J., Fan, W., Luo, M., and Zhang, L.: Contributions of External Forcing
885 and Internal Climate Variability to Changes in the Summer Surface Air Temperature over East Asia, *Journal of*
886 *Climate*, 35, 5013–5032, <https://doi.org/10.1175/JCLI-D-21-0577.1>, 2022.
- 887 Zhang, P., Yang, S., and Kousky, V. E.: South Asian high and Asian-Pacific-American climate teleconnection, *Advances*
888 *in Atmospheric Sciences*, <https://doi.org/10.1007/bf02918690>, 2005.
- 889 Zhang, S., Stier, P., and Watson-Parris, D.: On the contribution of fast and slow responses to precipitation changes caused
890 by aerosol perturbations, *Atmospheric Chemistry and Physics*, <https://doi.org/10.5194/acp-21-10179-2021>, 2021.
- 891 Zhou, S., Huang, P., Huang, G., and Hu, K.: Leading source and constraint on the systematic spread of the changes in
892 East Asian and western North Pacific summer monsoon, *Environmental Research Letters*,
893 <https://doi.org/10.1088/1748-9326/ab547c>, 2019.
- 894 Zhou, Z. Q. and Xie, S. P.: Effects of climatological model biases on the projection of tropical climate change, *Journal of*
895 *Climate*, <https://doi.org/10.1175/JCLI-D-15-0243.1>, 2015.
- 896



897 Table 1. Model simulations carried out in this study. The Asia domain (10°–45°N, 60°–125°E) is enclosed by the purple box in Fig.
898 1c. Note wind nudging is applied only above the planetary boundary layer (model level 12, or approximately 850 hPa). Years 2003 –
899 2012 are used for analysis.

Experiment	Description
CONT	Transient Asian aerosols during 1991–2012 and without nudging
CONTfA	Asian aerosols fixed at their 1991 values and without nudging
NUDG	Same as CONT except for wind nudging outside Asia
NUDGfA	Same as CONTfA except for wind nudging outside Asia

900

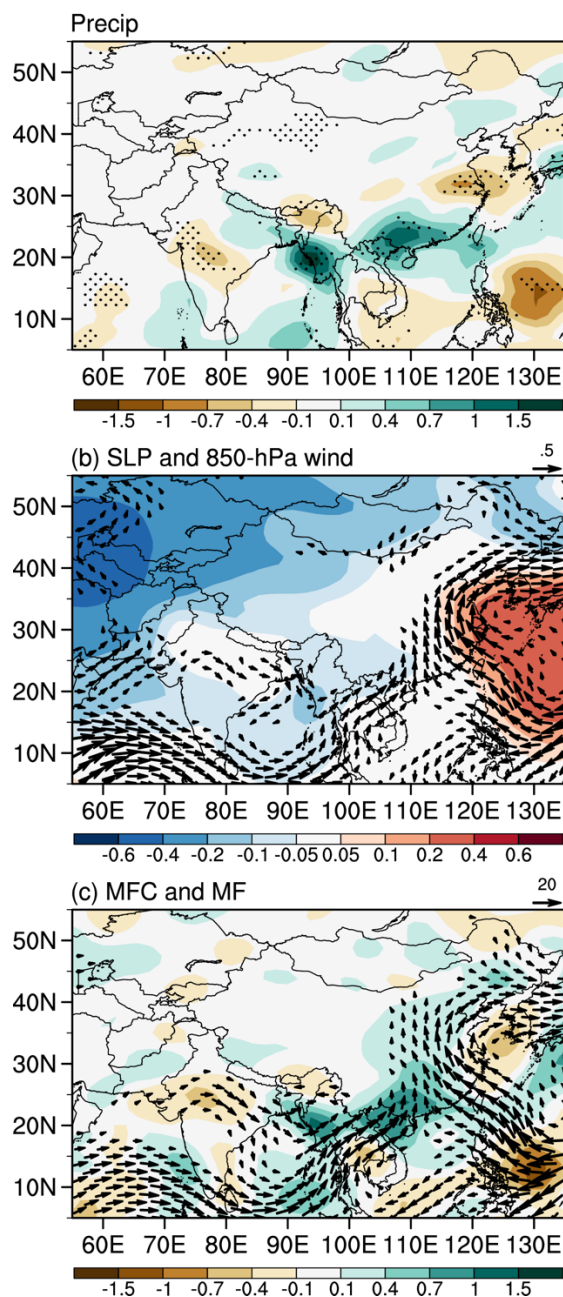


901

902 Fig. 1. (a) Differences of annual time series of summer AOD (unitless; red), total SO₂ emissions (Tg yr⁻¹; blue), total BC emissions
 903 (Tg yr⁻¹; black), total OC emissions (Tg yr⁻¹; brown), and total biomass burning emissions (Tg yr⁻¹; purple) over Asia between CONT
 904 and CONTfA. Spatial distribution of (b) SO₂ emissions (shading; Tg yr⁻¹) and sulfate column burden (contour; mg m⁻²) and (c) AOD
 905 changes (difference between CONT and CONTfA averaged for the period 2003–2012). The purple box in (c) denotes the Asia region
 906 (10°–45°N, 60°–125°E). Black dots in (c) mark grid-points for which the difference is significant at the 90% confidence level.

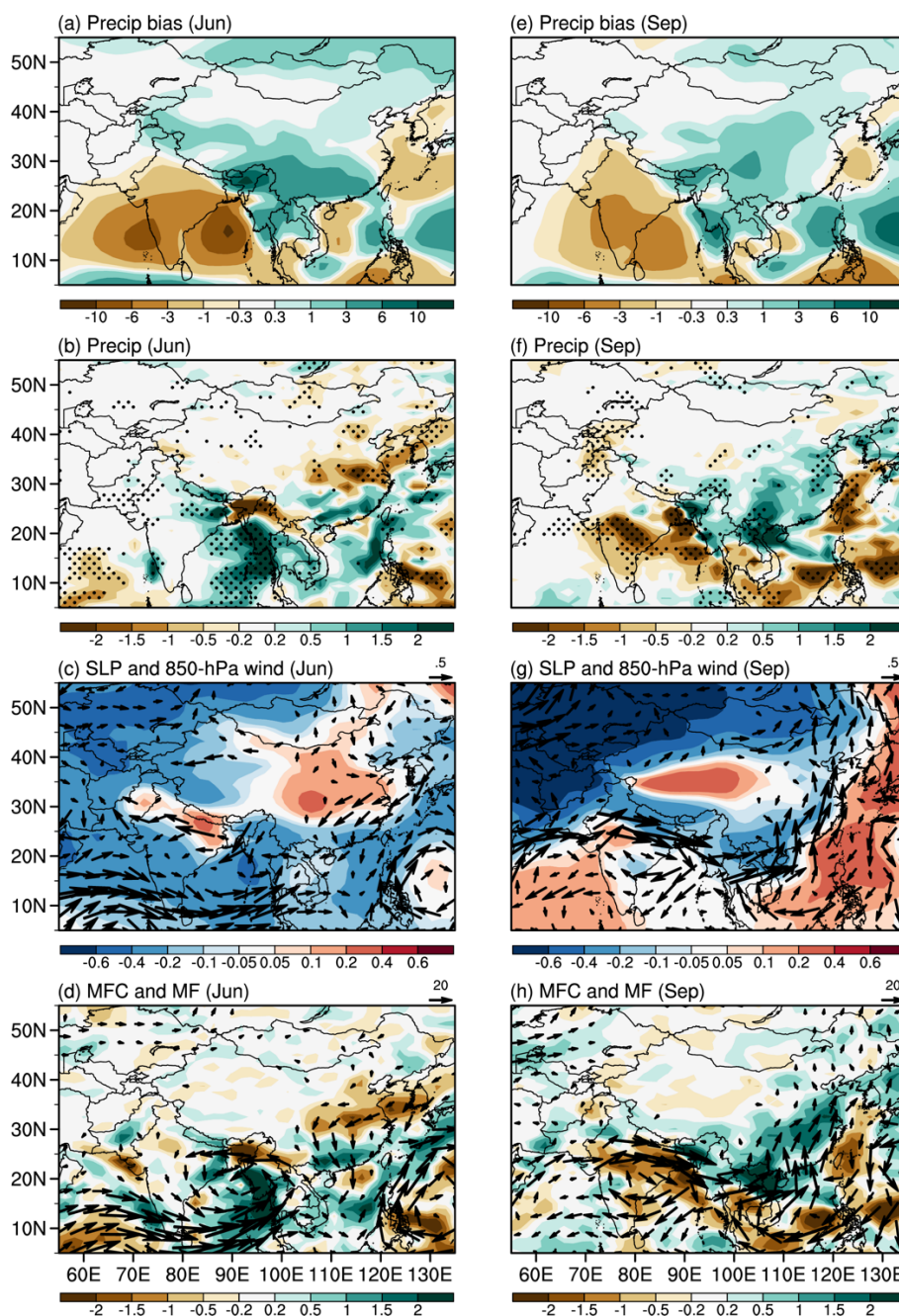


CONT - CONTfA (JJAS)



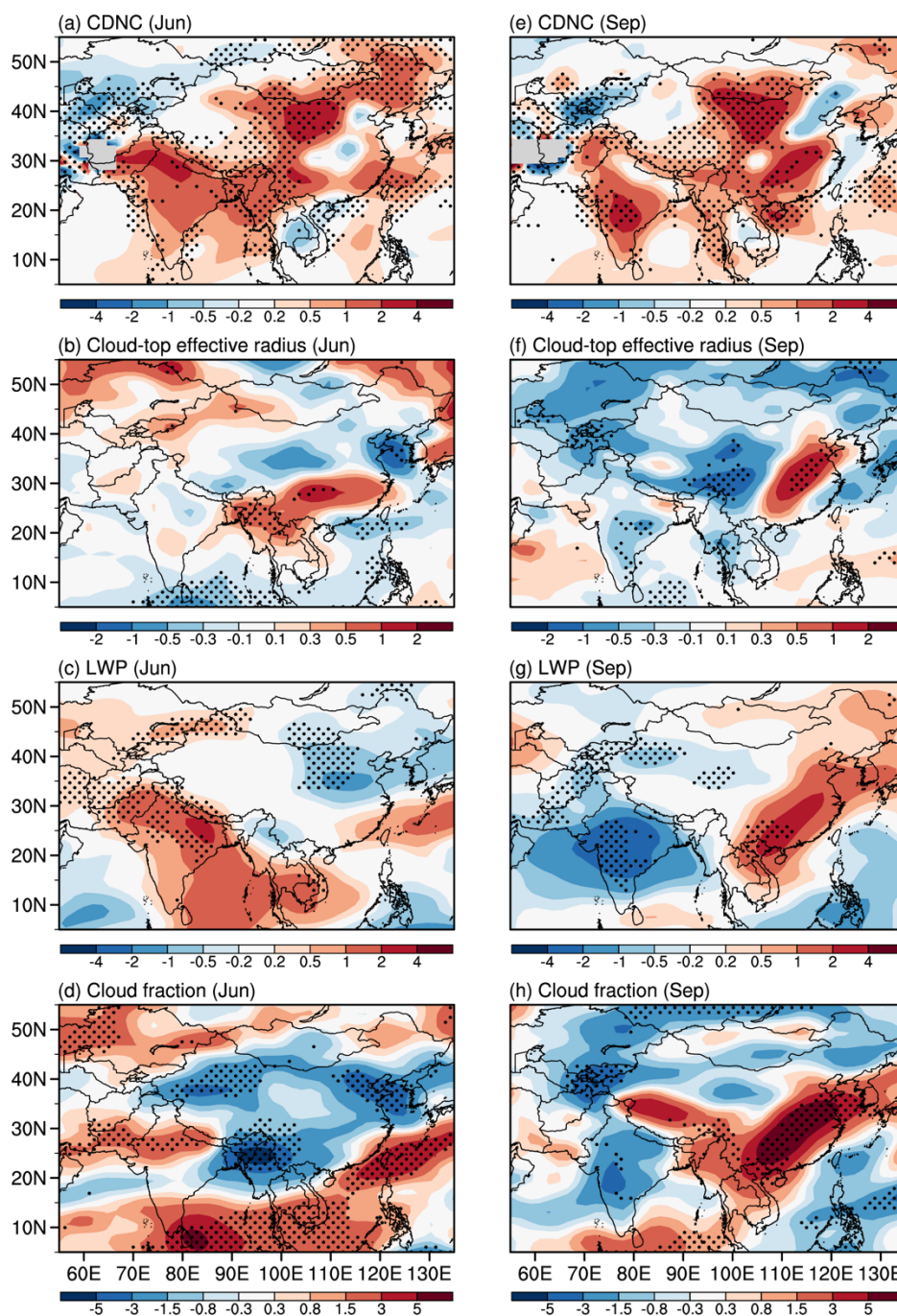
907

908 Fig. 2. JJAS response to Asian anthropogenic aerosols (difference between CONT and CONTfA averaged during 2003-2012) for (a)
909 precipitation (mm day^{-1}), (b) sea-level pressure (hPa; shades) and 850-hPa winds (m s^{-1}), and (c) 1000–300 hPa vertically integrated
910 moisture flux convergence (mm day^{-1} , shades) and moisture flux ($\text{kg m}^{-1} \text{s}^{-1}$). Black dots in (a) mark grid-points for which the difference
911 is significant at the 90% confidence level.

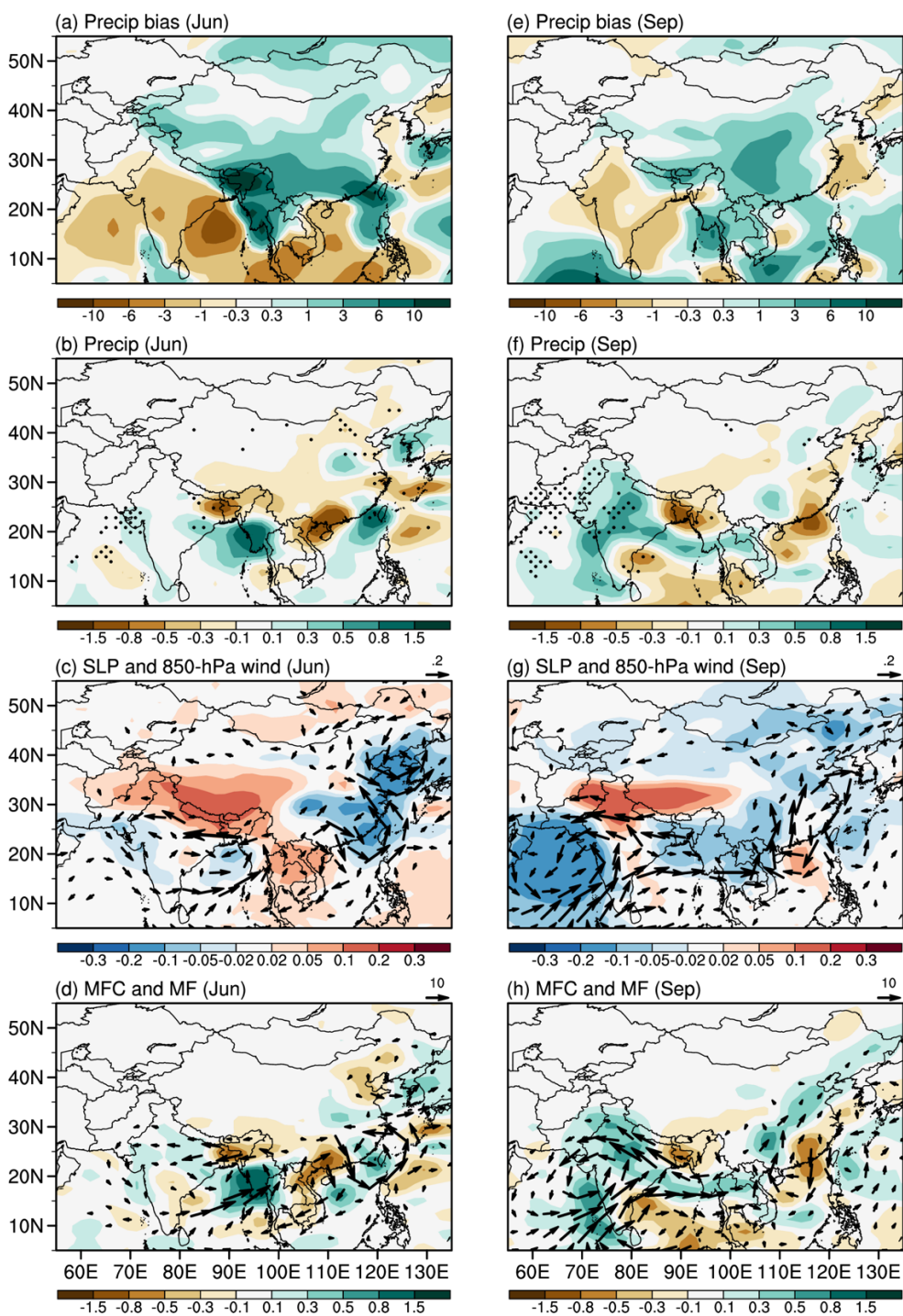


912

913 Fig. 3. (a) June precipitation bias (mm day^{-1}) in CONT with respect to the mean of GPCP and CMAP. Model data are averaged over
 914 2003–2012, observations over 1981–2010. June response to Asian anthropogenic aerosols (difference between CONT and CONTfA
 915 averaged during 2003–2012) for (b) precipitation (mm day^{-1}), (c) sea-level pressure (hPa, shades) and 850-hPa wind (m s^{-1}), and (d)
 916 1000–300 hPa vertically integrated moisture flux convergence (mm day^{-1} , shades) and moisture flux ($\text{kg m}^{-1} \text{s}^{-1}$). (e–h) Same as (a–d)
 917 but for September. Black dots in (b) and (f) mark grid-points for which the difference is significant at the 90% confidence level.

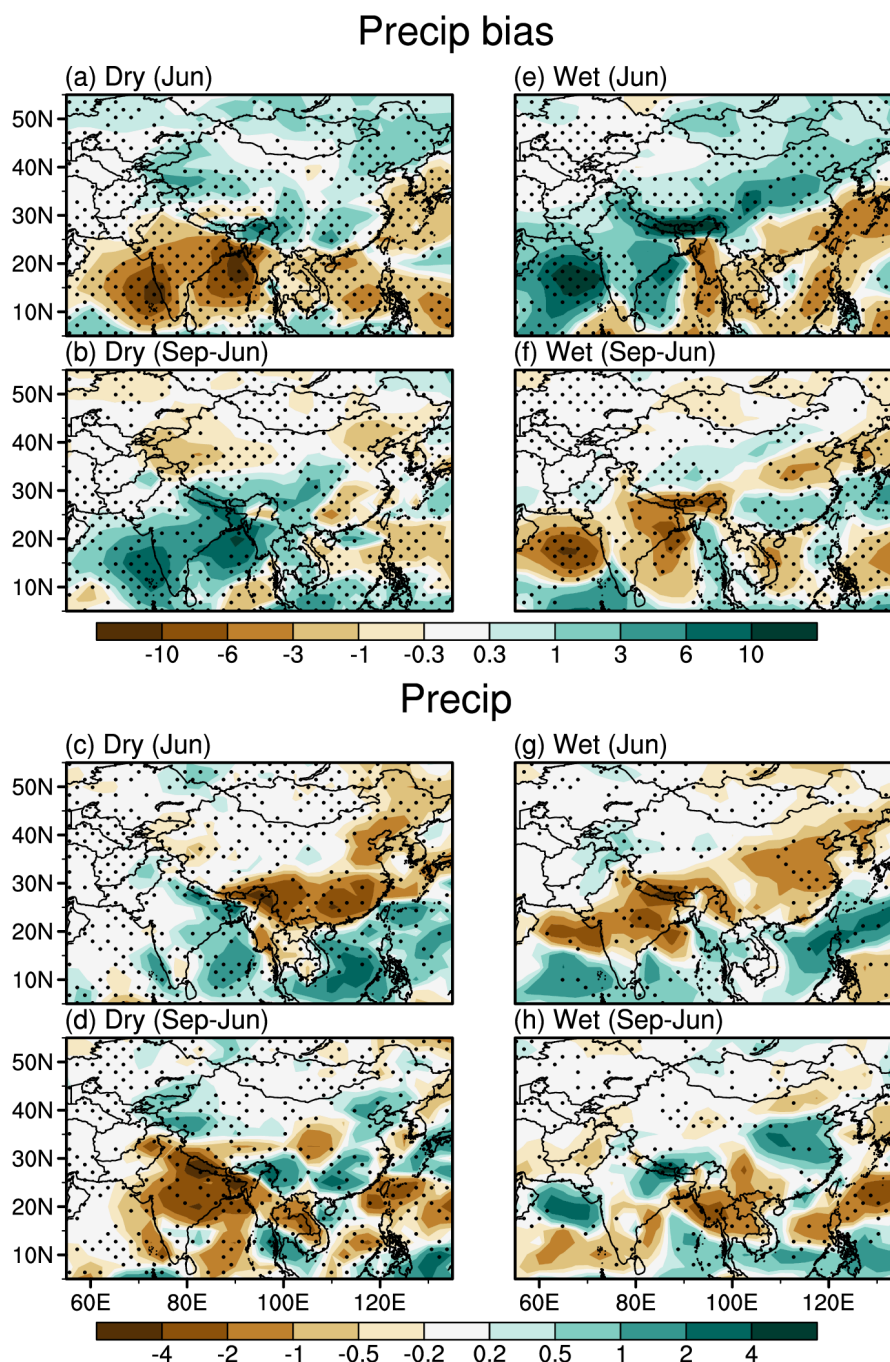


918
 919 Fig. 4. June response to Asian anthropogenic aerosols (difference between CONT and CONTfA averaged during 2003-2012) for (a)
 920 cloud droplet number concentration (10^{10} m^{-2}), (b) cloud-top effective radius (μm), (c) liquid water path (g m^{-2}), and (d) cloud fraction
 921 (%). (e-h) Same as (a-d) but for September. Black dots mark grid-points for which the difference is significant at the 90% confidence
 922 level.



923

924 Fig. 5. Same as Fig. 3 but for the difference between the corresponding nudged simulations (i.e., NUDG–NUDGFa).



925

926

927

928

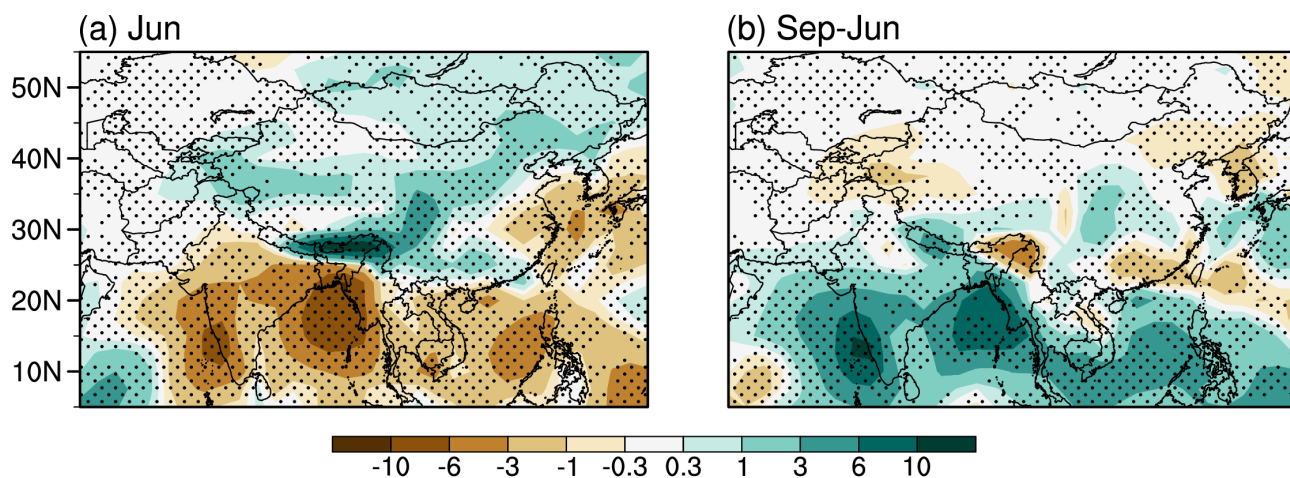
929

930

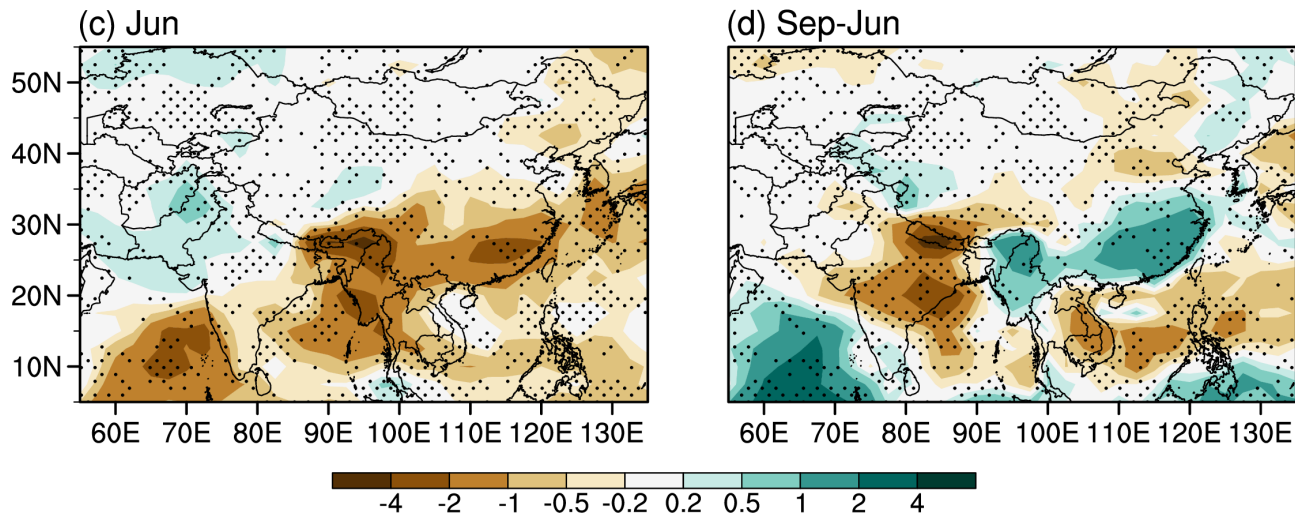
Fig. 6. DRY PDRMIP model composites in (a) June precipitation bias (mm day^{-1}), (b) September minus June difference in precipitation bias, (c) June precipitation response to increased Asian sulfate aerosols (i.e., the difference between $10\times$ sulfate and baseline simulations), and (d) September minus June difference in the precipitation response to increased Asian sulfate aerosols. (e–h) Same as (a–d) but for WET PDRMIP model composites. Black dots mark grid-points for which all models agree on the sign of the precipitation differences.



Precip bias



Precip

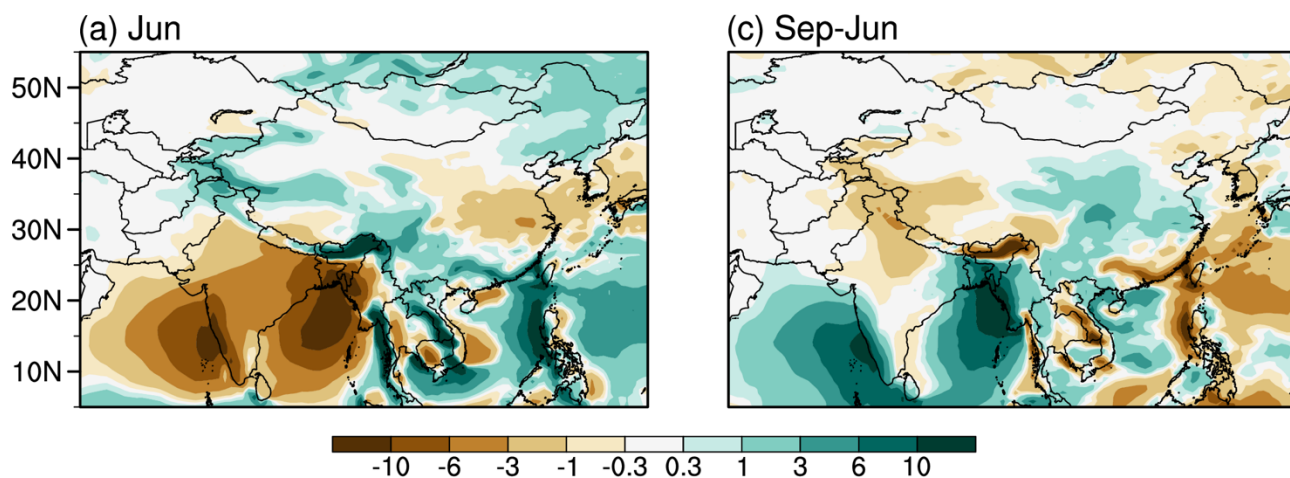


931

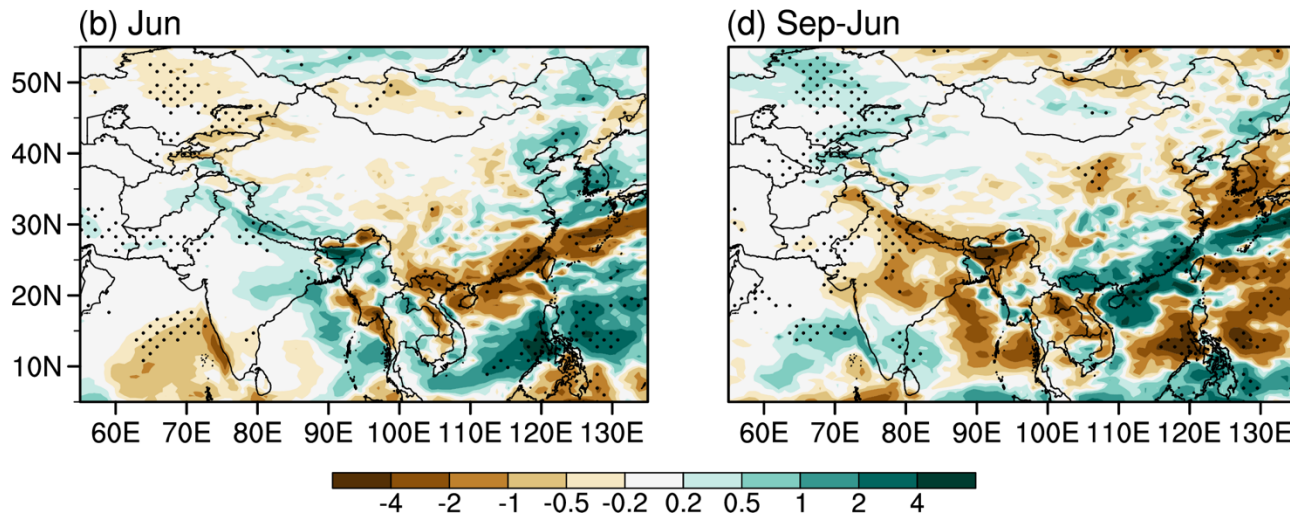
932 Fig. 7. PDRMIP coupled model composites in (a) June precipitation bias (mm day^{-1}), and (b) June precipitation response to increased
933 Asian sulfate aerosols (i.e., the difference between 10 \times sulfate and baseline simulations). (c)-(d): Same as (a)-(b) but for the September
934 minus June differences. Black dots mark grid-points for which at least four out of the five models agree on the sign of the precipitation
935 differences.



Precip bias



Precip



936

937 Fig. 8. (a) June precipitation bias (mm day^{-1}) in HadGEM3-GC2 coupled simulations, (b) precipitation bias difference between
938 September and June, (c) June precipitation response to Asian aerosol changes, (d) difference in the precipitation response to Asian
939 aerosols between September and June. Black dots in (b) and (d) mark grid-points for which the difference is significant at the 90%
940 confidence level.

941